^{129}Xe spin relaxation in frozen xenon

R. J. Fitzgerald,* M. Gatzke,† David C. Fox,‡ G. D. Cates, and W. Happer
Department of Physics, Princeton University, Princeton, New Jersey 08544
(Received 2 September 1998)

We discuss the longitudinal spin relaxation of ^{129}Xe nuclei in frozen xenon. Over a large range of temperatures and magnetic fields, the dominant spin-lattice relaxation mechanism is shown to be nuclear spin-flip Raman scattering of lattice phonons. Two closely related interactions couple the lattice phonons to the spins of ^{129}Xe nuclei: (1) the nuclear spin-rotation interaction between nearest-neighbor atoms, and (2) the paramagnetic antishielding of the externally applied field at the site of ^{129}Xe nuclei by the electrons of neighboring Xe atoms. We show that relaxation rates can be predicted by using measured chemical shifts of gaseous and condensed xenon. The predicted relaxation rates are in good agreement with measurements. We outline a simple way to estimate the spin-rotation coupling and paramagnetic antishielding in terms of the small perturbations of the outermost electron orbitals of one xenon atom due to a neighboring atom.
[S0163-1829(99)05513-7]

I. INTRODUCTION

Since the very earliest work on nuclear magnetic resonance,[1] it has been known that immobile spin-1/2 nuclei in diamagnetic crystals can have relaxation times of many hours. The observed relaxation is often due to paramagnetic impurities. Here we discuss the relaxation of the spin-1/2 isotope ^{129}Xe in frozen xenon. Because freezing excludes most impurities, intrinsic interactions characteristic of the pure xenon crystal could dominate the relaxation. We show that at applied magnetic fields above a few hundred gauss and at temperatures between about 20 and 120 K, the observed longitudinal relaxation time in frozen xenon is well described by nuclear spin-flip Raman scattering of phonons.

At magnetic fields between a few hundred and tens of thousands of gauss, the coupling is dominated by the phonon-induced spin-rotation interaction,

$$v = \frac{c_K}{\hbar}\mathbf{K}\cdot\mathsf{I}\cdot\boldsymbol{\omega} = c_K\mathbf{K}\cdot\mathbf{N}, \tag{1.1}$$

between the nuclear spin $\mathbf{K}$ of a ^{129}Xe atom and the angular momentum $\mathbf{N}$ of the ^{129}Xe atom and a nearest-neighbor atom rotating about each other with angular velocity $\boldsymbol{\omega}$. We use the notation of Ramsey[2,3] for the coupling coefficient $c_K = c_K(R)$, which depends on the internuclear separation R of the pair. As indicated in Eq. (1.1), the angular momentum $\mathbf{N}$ of the pair of atoms is related to their angular velocity $\boldsymbol{\omega}$ about each other by

$$\hbar\mathbf{N} = \mathsf{I}\cdot\boldsymbol{\omega}. \tag{1.2}$$

The inertial tensor I of a pair of xenon atoms, displaced from each other by $\mathbf{R}$, is

$$\mathsf{I} = \frac{M}{2}(R^2\mathbf{1} - \mathbf{RR}), \tag{1.3}$$

where M is the mass of a xenon atom and $\mathbf{1} = \mathbf{xx} + \mathbf{yy} + \mathbf{zz}$ is the unit dyadic constructed from the Cartesian unit vectors $\mathbf{x}$, $\mathbf{y}$, and $\mathbf{z}$. The relaxation of ^{129}Xe nuclear spins in pure, high-pressure xenon gas and in xenon liquid is believed to be due to the interaction (1.1).[4,5]

At fields of a few hundred thousand gauss, a very sizable contribution to the spin relaxation should also come from phonon-induced fluctuations of the paramagnetic antishielding interaction

$$v' = \frac{c_K}{\hbar}\mathbf{K}\cdot\mathsf{I}\cdot\boldsymbol{\omega}_0. \tag{1.4}$$

The Larmor frequency of an electron in the applied magnetic field $\mathbf{B}_0$ is $\boldsymbol{\omega}_0 = e\mathbf{B}_0/2mc$, and the coupling coefficient c_K is the same as in Eq. (1.1).

In Sec. II, we show that the closely related interactions (1.1) and (1.4), which act simultaneously in the crystal, have the largest influence on spin relaxation by causing Raman scattering of phonons.[6] In an analysis similar to that of van Kranendonk for Raman scattering of phonons by the nuclear quadrupole interaction,[7] we find that the spin-rotation interaction (1.1) leads to a longitudinal relaxation rate

$$\frac{1}{T_1^S} = \frac{9\pi c_{K0}^2 T^{*2}}{4\hbar^2\omega_D}\eta^S(\epsilon_0, T^*). \tag{1.5}$$

The paramagnetic antishielding interaction (1.4) makes an analogous contribution to the relaxation rate,

$$\frac{1}{T_1^P} = \frac{9\pi c_{K0}^2 T^{*2}}{4\hbar^2\omega_D}\left(\frac{\omega_0}{\omega_D}\right)^2\eta^P(\epsilon_0, T^*). \tag{1.6}$$

The relative temperature $T^* = T/T_D$ is the ratio of the crystal temperature T to the Debye temperature T_D [55 K for Xe (Ref. 8)], and $\omega_D = k_B T_D/\hbar$ is the Debye frequency. We will use the dimensionless function $\epsilon = \epsilon(R)$, defined by

$$\epsilon = R\frac{d}{dR}\ln c_K, \tag{1.7}$$

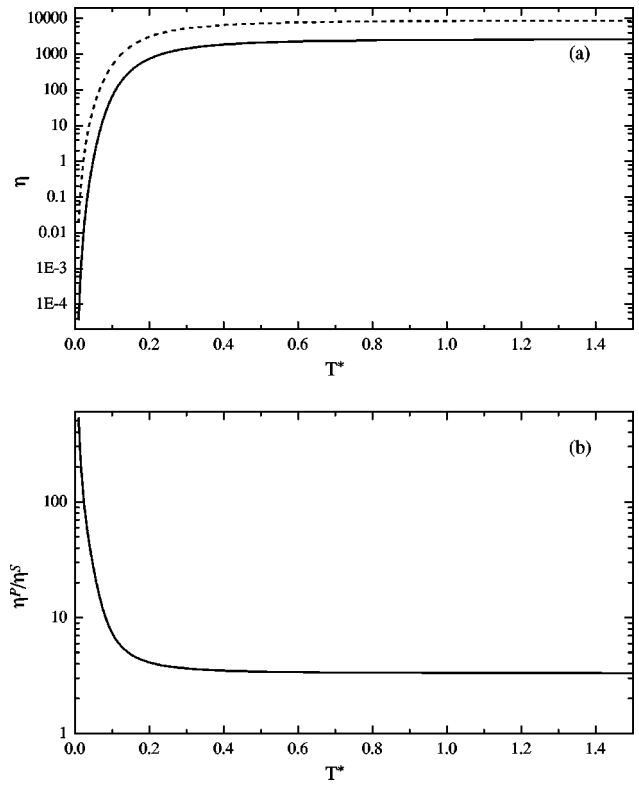

FIG. 1. (a) The efficiency functions $\eta^S(\epsilon_0, T^*)$ (solid line) and $\eta^P(\epsilon_0, T^*)$ (dashed line) parametrize the relaxation due to spin-flip Raman scattering of phonons through the spin-rotation interaction (1.1) and the paramagnetic antishielding interaction (1.4), respectively. $T^* = T/T_D$ is the ratio of the crystal temperature T to the Debye temperature T_D. The functions η^S and η^P asymptotically approach the constants 2686.8 and 8874.1 in solid Xe, using our estimate $\epsilon_0 = -11.8$ from Eq. (4.32) to characterize the variation in the coupling strength $c_K(R)$ with internuclear separation R. (b) The ratio η^P/η^S of the efficiencies, multiplied by the field-dependent factor $(B_0/B_D)^2$, gives the relative contributions of the paramagnetic antishielding and spin-rotation interactions to the relaxation rate. B_D is the field for which the electron Larmor frequency ω_0 equals the Debye frequency ω_D.

to characterize the rate of change of c_K with increasing internuclear separation R. At the equilibrium separation R_0 of nearest-neighbor xenon atoms in the crystal, $c_{K0} = c_K(R_0)$ and $\epsilon_0 = \epsilon(R_0)$. As in van Kranendonk's analysis,[7] the dimensionless efficiency functions $\eta^S(\epsilon_0, T^*)$ and $\eta^P(\epsilon_0, T^*)$, defined below by Eqs. (2.42) and (2.47), account for the ''freezing out'' of phonons at low temperatures, and are plotted in Fig. 1(a) using representative parameters for solid xenon.

Building on Ramsey's theory[2] of the chemical shift in molecules, Torrey[5] pointed out a close connection between the spin-rotation interaction (1.1) and the chemical shift σ of the nuclear magnetic resonance frequencies. The magnetic field $\mathbf{B}$ acting on a nucleus in a diamagnetic medium is often slightly smaller than the externally applied magnetic field $\mathbf{B}_0$ because of shielding currents of the surrounding electrons. The chemical shift tensor $\boldsymbol{\sigma}$ is defined by

$$\mathbf{B} = (\mathbf{1} - \boldsymbol{\sigma}) \cdot \mathbf{B}_0 . \tag{1.8}$$

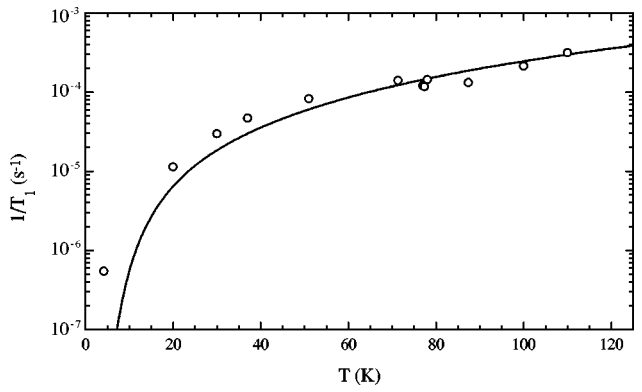

FIG. 2. Longitudinal relaxation rate $1/T_1$ of ^{129}Xe in frozen xenon as a function of temperature. The open circles are measured values of the longitudinal relaxation rate at an applied magnetic field (typically 1000–2000 G) large enough to eliminate field-dependent relaxation. The solid line is the rate (1.5), which would be expected if the spin relaxation were solely due to Raman scattering of phonons by the spin-rotation interaction (1.1) in frozen xenon. At these fields, the relaxation rate (1.6) due to fluctuations of the paramagnetic antishielding (1.4) is negligible.

In Sec. III we show that the spin-rotation coupling coefficient c_{K0} is related to the isotropic chemical shifts σ_g of gaseous xenon and σ_c of crystalline xenon by

$$\frac{c_{K0}}{h} = \left(\frac{\mu_K}{K\mu_B}\right)\left(\frac{\hbar}{8\pi M R_0^2}\right)(\sigma_g - \sigma_c), \tag{1.9}$$

where $\mu_B = e\hbar/(2mc)$ is the Bohr magneton, μ_K is the magnetic moment of the ^{129}Xe nucleus, $K = 1/2$ is the spin of the nucleus, and M is the mass of a xenon atom. We have used Eq. (1.9) along with recent measurements of the chemical shifts of gaseous and crystalline xenon[9] to determine $c_{K0}/h = -27$ Hz. Using this value of c_{K0}, together with an estimate of $\epsilon_0 = -11.8$ at $R_0 = 4.4$ Å, as derived in Sec. IV, we have evaluated the predicted rate (1.5) and compared it with our measurements of the longitudinal relaxation rate $1/T_1$ in Fig. 2.

The excellent agreement between measurements[10–12] and theory illustrated by Fig. 2 shows that Raman scattering of phonons through the spin-rotation interaction (1.1) is a limiting relaxation mechanism for ^{129}Xe in frozen xenon for temperatures between 20 and 120 K. For $T \gtrsim 120$ K, the relaxation due to diffusion of vacancies is no longer negligible;[8,13] for $T \lesssim 20$ K, the ^{129}Xe polarization lifetime appears to be limited by cross relaxation to ^{131}Xe, as discussed below in Sec. V.

Norberg and his collaborators[8] have already shown that an analogous intrinsic relaxation mechanism, Raman scattering of phonons through the nuclear quadrupole interaction, is responsible for the spin-lattice relaxation of ^{131}Xe in solid xenon. The quadrupole interaction is much more potent than the spin-rotation interaction. For example, at 30 K and for fields $B_0 > 1000$ G, the spin-lattice relaxation time of ^{131}Xe is[8] ~ 10 s, while the spin-lattice relaxation time of ^{129}Xe is[11] $\sim 50\,000$ s.

The spin-rotation interaction (1.1), which leads to the relaxation rate (1.5), and fluctuations in the paramagnetic antishielding (1.4), which leads to the relaxation rate (1.6), are

closely related to the mechanisms[14] responsible for spin relaxation of ^{13}C in liquid CS_2. Relaxation due to magnetic dipole interactions between ^{13}C spins is negligible, and the relaxation is dominated by the spin-rotation interaction of the tumbling CS_2 molecules, with a smaller but noticeable contribution at high applied magnetic fields from fluctuations in the diamagnetic shielding.[15] The anisotropic shielding fluctuates for ^{13}C as the molecule reorients in the liquid. This causes the magnetic field experienced by each ^{13}C nucleus to fluctuate, and makes a contribution to the spin-relaxation rate. For xenon ice at temperatures well below the melting temperature, where effects of vacancy diffusion are neglible, the modulation of the paramagnetic antishielding by phonons plays the same role as reorientation of CS_2 molecules. Because of this different physical origin for the fluctuations, the relaxation rates depend differently on the temperature for ^{13}C in liquid CS_2 and for ^{129}Xe in xenon ice. At temperatures comparable to the Debye temperature, the relaxation rate of ^{129}Xe is predicted to increase with the square of the temperature for both the spin-rotation interaction (1.5) and the antishielding interaction (1.6). For ^{13}C in liquid CS_2, the spin-rotation contribution to the rate increases with increasing temperature, but the contribution to the rate from the anisotropic shielding decreases. For both liquid CS_2 and xenon ice, the contributions to the relaxation rate from the fluctuating shielding are proportional to B_0^2.

As Ramsey[2] pointed out, the spin-rotation coupling coefficient c_K and the related change in the chemical shift for condensed xenon are mainly due to the ''paramagnetic'' electron currents. These can be generated by an applied magnetic field or by the relative motion of contiguous xenon atoms when no applied field is present. In Sec. IV, we use the simple pseudopotential method of Wu *et al.*[16] to derive an expression for c_K,

$$\frac{c_K}{h}=\frac{-2\mu_K e}{\pi KMc}|f|^2\left\langle\frac{1}{r^3}\right\rangle S^{(1)}(S^{(1)}+S^{(3)}). \tag{1.10}$$

Here e is the magnitude of the electron charge, c is the speed of light, and $\langle 1/r^3\rangle$ is the expectation value of $1/r^3$ for a $5p$ electron in an isolated xenon atom displaced a distance r from the nucleus. The dimensionless parameter f, which can be taken to be $f=1$ as a first approximation, is a gauge of how much the admixture coefficients for the wave functions differ from the values obtained from simple orthogonalization. $S^{(1)}$ and $S^{(3)}$, defined below by Eqs. (4.17) and (4.18), are π and σ overlap integrals of $5p$ wave functions. The orthogonalization method leading to Eq. (1.10) gives estimates which agree as well with experiment as, and are much simpler to calculate than, those obtained by the usual second-order perturbation method introduced by Ramsey,[2] where a sum over multicenter intermediate states must be evaluated.[17] Since the orthogonalization method is closely related to well-developed pseudopotential methods for condensed-matter physics,[18] it is amenable to straightforward improvement.

In Sec. V we describe the experiments[10] used to obtain the data of Fig. 2. The experimental measurements were facilitated by the use of spin-exchange laser pumping of xenon gas mixed with alkali metal vapor. The gas was subsequently frozen. This allowed us to work with samples which had many orders of magnitude higher nuclear spin polarization than at thermal equilibrium. Chemical scavenging of residual oxygen gas and other impurities by the alkali metal ensured that the frozen xenon samples were of high purity.

An important check on the basic physics underlying this work would be a measurement of the spin-relaxation rate of ^{129}Xe at very high magnetic fields, where the relaxation rate (1.6) due to fluctuations in the paramagnetic antishielding is comparable to the rate (1.5) due to the spin-rotation interaction.

II. SPIN-FLIP SCATTERING OF PHONONS

We will describe a solid xenon crystal with a simple Debye model, with a common speed of sound c_s for longitudinal and transverse phonons.[6] We can write the position $\mathbf{R}_\nu$ of atom ν as the sum of its equilibrium position $\mathbf{R}_\nu^{(0)}$ and a displacement from equilibrium $\mathbf{S}_\nu$:

$$\mathbf{R}_\nu=\mathbf{R}_\nu^{(0)}+\mathbf{S}_\nu. \tag{2.1}$$

The displacement $\mathbf{S}_\nu$ will fluctuate because of thermal vibrations of the lattice and also because of the zero-point excitations of the phonons.

We can write the displacement as a superposition of the creation operators $a_{\mathbf{k}j}^\dagger$ and annihilation operators $a_{\mathbf{k}j}$ of phonons of momentum $\hbar\mathbf{k}$, vibrating along the direction of the unit vector $\mathbf{x}_j$. Because of our assumption of a common speed of sound for longitudinal and transverse phonons, one of the polarization unit vectors $\mathbf{x}_3=\mathbf{z}=\mathbf{B}_0/B_0$ can be chosen to be parallel to the externally applied magnetic field $\mathbf{B}_0$, and two additional unit vectors $\mathbf{x}_1=\mathbf{x}$ and $\mathbf{x}_2=\mathbf{y}$ can be chosen to make an orthonormal, Cartesian basis. Then the displacement operator for atom ν is

$$\mathbf{S}_\nu=\sqrt{\frac{\hbar}{2NMc_s}}\sum_{\mathbf{k}j}\frac{\mathbf{x}_j a_{\mathbf{k}j}}{\sqrt{k}}e^{i\mathbf{k}\cdot\mathbf{R}_\nu}+\text{H.c.}, \tag{2.2}$$

and the momentum operator is

$$\mathbf{P}_\nu=-i\sqrt{\frac{\hbar Mc_s}{2N}}\sum_{\mathbf{k}j}\sqrt{k}\,\mathbf{x}_j a_{\mathbf{k}j}e^{i\mathbf{k}\cdot\mathbf{R}_\nu}+\text{H.c.} \tag{2.3}$$

We denote the Hermitian conjugate of the sums in Eqs. (2.2) and (2.3) by ''H.c.''

The sums (2.2) and (2.3) extend over phonon plane waves of momentum $\hbar\mathbf{k}$ and over the three mutually orthogonal unit vectors $\mathbf{x}_j$ of the phonon polarization. The crystal has a volume V and is composed of N atoms, each with mass M. A crystal with N atoms will have N phonon states of a given polarization. Each phonon state takes up a volume $8\pi^3/V$ in wave number space. The density of states in wave number space is uniform within a sphere of radius k_D and there are no states with wave numbers larger than k_D. The Debye wave number k_D, the Debye frequency ω_D, the Debye energy E_D, and the Debye temperature T_D are related to the atomic number density of the crystal by

$$k_D=\frac{\omega_D}{c_s}=\frac{E_D}{\hbar c_s}=\frac{k_B T_D}{\hbar c_s}=\left(\frac{6\pi^2 N}{V}\right)^{1/3}, \tag{2.4}$$

where k_B is Boltzmann's constant. The phonon energy E is related to the magnitude of the phonon momentum $\hbar k$ by

$$E=\hbar c_s k. \tag{2.5}$$

The number of phonon states of a specific polarization per unit energy and per unit solid angle is, therefore,

$$\rho(E)=\begin{cases} 3NE^2/(4\pi E_D^3), & E<E_D; \\ 0, & E>E_D. \end{cases} \tag{2.6}$$

Let $|n_{\mathbf{k}j}\rangle$ be a basis state of the vibrating crystal with $n_{\mathbf{k}j}$ phonons of momentum $\hbar\mathbf{k}$ and polarization $\mathbf{x}_j$. Operating on such a state, the phonon annihilation operator $a_{\mathbf{k}j}$ eliminates one phonon,

$$a_{\mathbf{k}j}|n_{\mathbf{k}j}\rangle=\sqrt{n_{\mathbf{k}j}}\,|n_{\mathbf{k}j}-1\rangle. \tag{2.7}$$

In like manner, the phonon creation operator $a_{\mathbf{k}j}^\dagger$ increases the phonon occupation number by one,

$$a_{\mathbf{k}j}^\dagger|n_{\mathbf{k}j}\rangle=\sqrt{n_{\mathbf{k}j}+1}\,|n_{\mathbf{k}j}+1\rangle. \tag{2.8}$$

The nuclear spin $\mathbf{K}$ of atom α will interact with the lattice through pairwise spin-rotation couplings to each nearest-neighbor atom β. Let $\mathbf{N}_{\beta\alpha}$ be the angular momentum (in units of $\hbar$) of atom β and atom α about their center of mass. The spin-rotation interaction is

$$v=\sum_\beta c_K(R_{\beta\alpha})\mathbf{N}_{\beta\alpha}\cdot\mathbf{K}=\frac{1}{2\hbar}\sum_\beta c_K(R_{\beta\alpha})\mathbf{R}_{\beta\alpha}\times\mathbf{P}_{\beta\alpha}\cdot\mathbf{K}$$
$$=v^{(1)}+v^{(2)}+\cdots, \tag{2.9}$$

where

$$\mathbf{P}_{\beta\alpha}=\mathbf{P}_\beta-\mathbf{P}_\alpha \tag{2.10}$$

is the difference in the linear momenta of atom β and atom α. Following Eq. (2.1), we write the distance from the atom α to atom β as

$$\mathbf{R}_{\beta\alpha}=\mathbf{R}_{\beta\alpha}^{(0)}+\mathbf{S}_{\beta\alpha}, \tag{2.11}$$

where $\mathbf{R}_{\beta\alpha}^{(0)}$ is the difference in the equilibrium positions

$$\mathbf{R}_{\beta\alpha}^{(0)}=\mathbf{R}_\beta^{(0)}-\mathbf{R}_\alpha^{(0)}, \tag{2.12}$$

and $\mathbf{S}_{\beta\alpha}$ is the difference between the displacements

$$\mathbf{S}_{\beta\alpha}=\mathbf{S}_\beta-\mathbf{S}_\alpha. \tag{2.13}$$

The nuclear spin $\mathbf{K}$ of atom α will also couple to the lattice through the contribution to the chemical shift of paramagnetic antishielding currents from neighboring atoms. The potential for this interaction is

$$v'=\sum_\beta c_K(R_{\beta\alpha})\boldsymbol{\omega}_0\cdot\mathsf{I}\cdot\mathbf{K}=\frac{M}{2\hbar}\sum_\beta c_K(R_{\beta\alpha})$$
$$\times\boldsymbol{\omega}_0\cdot(R_{\beta\alpha}^2\mathbf{1}-\mathbf{R}_{\beta\alpha}\mathbf{R}_{\beta\alpha})\cdot\mathbf{K}=v'^{(1)}+v'^{(2)}+\cdots. \tag{2.14}$$

Since xenon freezes as a face-centered-cubic crystal, there will be 12 terms in the sum over nearest-neighbors atoms β in Eqs. (2.9) and (2.14), as sketched in Fig. 3. As we discuss in Sec. IV, the coupling coefficient $c_K(R)$ decreases so rapidly with increasing R that only nearest-neighbor interactions need be considered.

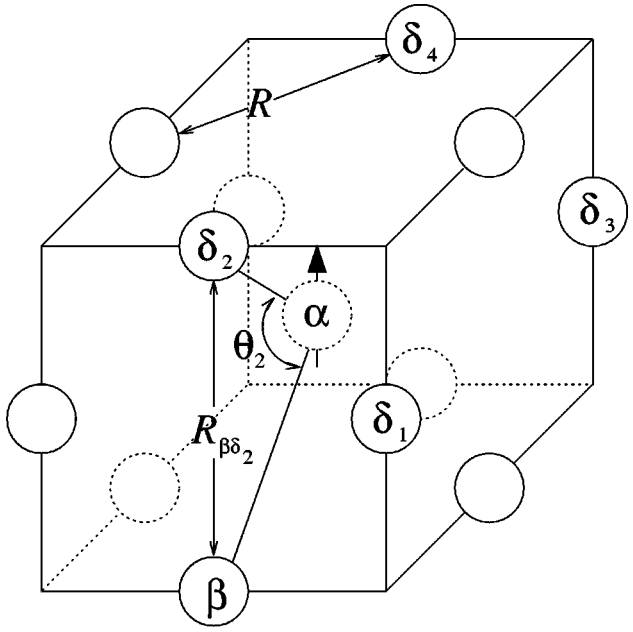

FIG. 3. The 12 nearest neighbors of a spin-up ^{129}Xe atom α. As summarized in Table I, the ordered pairs of nearest neighbors can be partitioned into five sets Λ_m, with $m=0,1,2,3,4$. Pairs of atoms in the same set subtend the same angle θ_m at the central atom α. The pairs (β,δ_m) for $m=1,2,3,4$ are examples of members of the sets Λ_m. The 12 nearest-neighbor atoms paired with themselves compose the set Λ_0.

As indicated in Eqs. (2.9) and (2.14), the spin-rotation and paramagnetic antishielding interactions can be decomposed into n-phonon components: $v^{(n)}$ and $v'^{(n)}$ contain terms which can absorb n phonons, or absorb $n-1$ phonons and emit 1 phonon, or absorb $n-2$ phonons and emit 2 phonons, etc. To obtain this series, we use a power-series expansion of c_K,

$$c_K(R_{\beta\alpha})=c_{K0}\left\{1+\frac{\epsilon_0}{R_0^2}\mathbf{S}_{\beta\alpha}\cdot\mathbf{R}_{\beta\alpha}^{(0)}+\frac{\epsilon_0}{2}\left[\frac{S_{\beta\alpha}^2}{R_0^2}+(\epsilon_0-1)\right.\right.$$
$$\left.\left.\times\frac{(\mathbf{S}_{\beta\alpha}\cdot\mathbf{R}_{\beta\alpha}^{(0)})^2}{R_0^4}\right]+\cdots\right\}, \tag{2.15}$$

about the equilibrium separation $R_0=|R_{\beta\alpha}^{(0)}|$, with $c_{K0}=c_K(R_0)$ and $\epsilon_0=\epsilon(R_0)$.

Using the expansion (2.15) together with Eq. (2.11) in Eqs. (2.9) and (2.14), we find that the one-phonon interactions are

$$v^{(1)}=\frac{c_{K0}}{2\hbar}\sum_\beta \mathbf{R}_{\beta\alpha}^{(0)}\times\mathbf{P}_{\beta\alpha}\cdot\mathbf{K} \tag{2.16}$$

and

$$v'^{(1)} = \frac{Mc_{K0}}{2\hbar}\sum_{\beta}\ \boldsymbol{\omega}_0\cdot\left[\frac{\epsilon_0}{R_0^2}\mathbf{S}_{\beta\alpha}\cdot\mathbf{R}^{(0)}_{\beta\alpha}(R_0^2\mathbf{1}-\mathbf{R}^{(0)}_{\beta\alpha}\mathbf{R}^{(0)}_{\beta\alpha}) + 2\mathbf{S}_{\beta\alpha}\cdot\mathbf{R}^{(0)}_{\beta\alpha}\mathbf{1}-\mathbf{S}_{\beta\alpha}\mathbf{R}^{(0)}_{\beta\alpha}-\mathbf{R}^{(0)}_{\beta\alpha}\mathbf{S}_{\beta\alpha}\right]\cdot\mathbf{K}. \quad (2.17)$$

The interactions (2.16) and (2.17) can cause the nuclear spin to flip with the emission or absorption of a single phonon. The two-phonon interactions are

$$v^{(2)}=\frac{c_{K0}}{2\hbar}\sum_{\beta}\ \left(\mathbf{S}_{\beta\alpha}\times\mathbf{P}_{\beta\alpha}+\frac{\epsilon_0}{R_0^2}\mathbf{S}_{\beta\alpha}\cdot\mathbf{R}^{(0)}_{\beta\alpha}\mathbf{R}^{(0)}_{\beta\alpha}\times\mathbf{P}_{\beta\alpha}\right)\cdot\mathbf{K} \quad (2.18)$$

and

$$v'^{(2)}=\frac{Mc_{K0}}{2\hbar}\sum_{\beta}\ \boldsymbol{\omega}_0\cdot\left\{S^2_{\beta\alpha}\mathbf{1}-\mathbf{S}_{\beta\alpha}\mathbf{S}_{\beta\alpha} + \frac{\epsilon_0}{R_0^2}\mathbf{R}^{(0)}_{\beta\alpha}\cdot\mathbf{S}_{\beta\alpha}(2\mathbf{S}_{\beta\alpha}\cdot\mathbf{R}^{(0)}_{\beta\alpha}\mathbf{1}-\mathbf{S}_{\beta\alpha}\mathbf{R}^{(0)}_{\beta\alpha}-\mathbf{R}^{(0)}_{\beta\alpha}\mathbf{S}_{\beta\alpha}) + \frac{\epsilon_0}{2}\left[\frac{S^2_{\beta\alpha}}{R_0^2}+(\epsilon_0-1)\frac{(\mathbf{S}_{\beta\alpha}\cdot\mathbf{R}^{(0)}_{\beta\alpha})^2}{R_0^4}\right] \times(R_0^2\mathbf{1}-\mathbf{R}^{(0)}_{\beta\alpha}\mathbf{R}^{(0)}_{\beta\alpha})\right\}\cdot\mathbf{K}. \quad (2.19)$$

The interactions (2.18) and (2.19) can cause the nuclear spin to flip with the emission of two phonons or the absorption of two phonons, or with the emission of one phonon and absorption of another (Raman scattering).

Except at impractically low crystal temperatures where the spin-relaxation times are so long as to be irrelevant, the single-phonon scattering described by Eqs. (2.16) and (2.17) make negligible contributions to the spin-relaxation rate in comparison to the Raman scattering described by Eqs. (2.18) and (2.19). All phonons in the lattice, and especially the very abundant phonons with energies $E\sim k_BT_D\sim10^{-14}$ erg, can contribute to Raman scattering, but single-phonon absorption or emission is possible only for the relatively few, extremely long-wavelength phonons with energies equal to the Zeeman energy $\mu_KB_0/K\sim10^{-20}$ erg of a nucleus of magnetic moment $\mu_K\sim10^{-24}$ erg/G in an applied magnetic field $B_0\sim10^4$ G. Furthermore, for the spin-rotation coupling, the long-wavelength phonons displace neighboring atoms by nearly the same amount and produce little of the relative momentum (2.10) needed for the one-phonon interaction (2.16). For similar reasons, the emission or absorption of two phonons during a spin-flip is negligible compared to Raman scattering. Thus, we will focus on relaxation processes for which the initial state,

$$|i\rangle=|m_K=1/2;\ \ldots,n_{\mathbf{k}_aj_a},n_{\mathbf{k}_ej_e},\ \ldots\rangle, \quad (2.20)$$

has the nuclear-spin projection $m_K=1/2$ and has $n_{\mathbf{k}_aj_a}$ phonons of momentum $\hbar\mathbf{k}_a$ and polarization $\mathbf{x}_{j_a}$ in the mode from which a phonon will be absorbed, and $n_{\mathbf{k}_ej_e}$ phonons of momentum $\hbar\mathbf{k}_e$ and polarization $\mathbf{x}_{j_e}$ in the mode into which a phonon will be emitted by Raman scattering. The final state,

$$|f\rangle=|m_K=-1/2;\ \ldots,n_{\mathbf{k}_aj_a}-1,n_{\mathbf{k}_ej_e}+1,\ \ldots\rangle, \quad (2.21)$$

has the nuclear-spin projection $m_K=-1/2$ and has $n_{\mathbf{k}_aj_a}-1$ and $n_{\mathbf{k}_ej_e}+1$ phonons in the respective modes.

According to Fermi's golden rule, the transition rate dW_{fi} from the initial state to final states for which a phonon is emitted within the solid angle $d\Omega_e$ is

$$dW_{fi}=\frac{2\pi}{\hbar}|v_{fi}|^2\rho(E_e)d\Omega_e. \quad (2.22)$$

The energy E_e of the emitted phonon differs from the energy E_a of the absorbed phonon by $|\mu_KB_0/K|\sim10^{-20}$ erg, the energy absorbed or released in a nuclear spin flip. This difference is negligible compared to the Debye energy $E_D\sim10^{-14}$ erg, which characterizes the phonon spectrum, and we therefore set $E_e=E_a$ in subsequent expressions. We integrate Eq. (2.22) over all directions of the emitted phonon and over all energies and directions of the absorbed phonon, and sum over the polarizations $\mathbf{x}_{j_e}$ and $\mathbf{x}_{j_a}$ of the emitted and absorbed phonons, to obtain the total rate of the transition $m_K=1/2$ to $m_K=-1/2$,

$$W_{fi}=\frac{2\pi}{\hbar}\sum_{j_ej_a}\int_0^{E_D}dE_a d\Omega_a d\Omega_e|v_{fi}|^2\rho^2(E_a). \quad (2.23)$$

We take the origin of the coordinate system to be the equilibrium position of atom α, so $\mathbf{R}^{(0)}_{\alpha}=0$. Then we find that the matrix element of Eq. (2.18) is

$$v^{(2)}_{fi}=\langle f|v^{(2)}|i\rangle=\frac{c_{K0}}{4Ni}\sqrt{n_a(n_e+1)}\sum_{\beta}\ (e^{-i\mathbf{k}_e\cdot\mathbf{R}^{(0)}_{\beta}}-1) \times(e^{i\mathbf{k}_a\cdot\mathbf{R}^{(0)}_{\beta}}-1)\,\mathbf{w}_{\beta}\cdot\mathbf{x}_+. \quad (2.24)$$

The unnormalized, circular basis vectors are

$$\mathbf{x}_{\pm}=\mathbf{x}\pm i\mathbf{y}. \quad (2.25)$$

The direction of the spin-flipping magnetic field, associated with the phonon-induced motion of the nearest-neighbor atom β, is defined by the vector

$$\mathbf{w}_{\beta}=\mathbf{x}_{j_e}\times\mathbf{x}_{j_a}+\frac{\epsilon_0}{2}(\mathbf{x}_{j_e}\cdot\mathbf{n}_{\beta}\mathbf{n}_{\beta}\times\mathbf{x}_{j_a}-\mathbf{x}_{j_a}\cdot\mathbf{n}_{\beta}\mathbf{n}_{\beta}\times\mathbf{x}_{j_e}), \quad (2.26)$$

with the unit vector from the origin (the nucleus α with $\mathbf{R}^{(0)}_{\alpha}=0$) to the nearest-neighbor atom β given by

$$\mathbf{n}_{\beta}=\mathbf{R}^{(0)}_{\beta}/R^{(0)}_{\beta}. \quad (2.27)$$

Similarly, the matrix element of Eq. (2.19) is

$$v'^{(2)}_{fi}=\langle f|v'^{(2)}|i\rangle=\frac{c_{K0}}{4N}\frac{E_D}{E_a}\sqrt{n_a(n_e+1)}\sum_{\beta}\ (e^{-i\mathbf{k}_e\cdot\mathbf{R}^{(0)}_{\beta}}-1) \times(e^{i\mathbf{k}_a\cdot\mathbf{R}^{(0)}_{\beta}}-1)\,\mathbf{w}'_{\beta}\cdot\mathbf{x}_+, \quad (2.28)$$

with

$$\mathbf{w}'_\beta=\frac{1}{2\omega_D}\boldsymbol{\omega}_0\cdot\{(\mathbf{x}_{j_e}\mathbf{x}_{j_a}+\mathbf{x}_{j_a}\mathbf{x}_{j_e})+\epsilon_0[\mathbf{n}_\beta\cdot\mathbf{x}_{j_e}(\mathbf{n}_\beta\mathbf{x}_{j_a}+\mathbf{x}_{j_a}\mathbf{n}_\beta)+\mathbf{n}_\beta\cdot\mathbf{x}_{j_a}(\mathbf{n}_\beta\mathbf{x}_{j_e}+\mathbf{x}_{j_e}\mathbf{n}_\beta)]+\epsilon_0[\mathbf{x}_{j_e}\cdot\mathbf{x}_{j_a}+(\epsilon_0-1)\times(\mathbf{n}_\beta\cdot\mathbf{x}_{j_e})(\mathbf{n}_\beta\cdot\mathbf{x}_{j_a})]\mathbf{n}_\beta\mathbf{n}_\beta\}. \tag{2.29}$$

The two Raman-scattering interactions (2.18) and (2.19) connect the same initial and final states (2.20) and (2.21) and thus their matrix elements add coherently. The relaxation due to the cross term between Eqs. (2.18) and (2.19) must vanish when the integrals of Eq. (2.23) are carried out, because such a cross term would be linear in $\mathbf{B}_0$, a behavior which is excluded by symmetry. Explicit calculations confirm that the contribution to Eq. (2.23) from the cross term vanishes.

We focus first on the spin-rotation interaction. Substituting Eq. (2.24) into Eq. (2.23) with $v_{fi}=v_{fi}^{(2)}$, and noting that the longitudinal relaxation time T_1 for a spin-1/2 nucleus is related to the transition rate (2.23) by

$$1/T_1=2W_{fi}, \tag{2.30}$$

we find

$$\frac{1}{T_1^S}=\frac{\pi c_{K0}^2}{4N^2\hbar}\sum_{\beta\delta}\sum_{j_e j_a}\int_0^{E_D}dE_a\,\rho^2(E_a)\,n_{\mathbf{k}_a j_a}(n_{\mathbf{k}_e j_e}+1)\times\mathbf{x}_+\cdot\mathbf{w}_\beta\mathbf{w}_\delta\cdot\mathbf{x}_-\times\int d\Omega_a\,(e^{i\mathbf{k}_a\cdot\mathbf{R}_\beta^{(0)}}-1)\times(e^{-i\mathbf{k}_a\cdot\mathbf{R}_\delta^{(0)}}-1)\times\int d\Omega_e\,(e^{i\mathbf{k}_e\cdot\mathbf{R}_\delta^{(0)}}-1)\times(e^{-i\mathbf{k}_e\cdot\mathbf{R}_\beta^{(0)}}-1). \tag{2.31}$$

The integrals over the angles of propagation of absorbed and emitted phonons can be carried out analytically, and we find for their average

$$\frac{1}{4\pi}\int d\Omega\,(e^{i\mathbf{k}\cdot\mathbf{R}_\beta^{(0)}}-1)(e^{-i\mathbf{k}\cdot\mathbf{R}_\delta^{(0)}}-1)=1+j_0(kR_{\beta\delta}^{(0)})-2j_0(kR_0). \tag{2.32}$$

The spherical Bessel functions (the ''sinc'' functions) of Eq. (2.32) are

$$j_0(x)=\frac{\sin x}{x}. \tag{2.33}$$

The sum over the 12 nearest neighbors β and 12 nearest neighbors δ in Eq. (2.31) gives 144 ordered pairs $\beta\delta$. From inspection of Fig. 3, we see that these can be divided into five sets Λ_m $(m=0,1,2,3,4)$ of g_m ordered pairs with the same separation

$$R_{\beta\delta}^{(0)}=\sigma_m R_0, \tag{2.34}$$

TABLE I. Nearest-neighbor pairs can be partitioned into five sets Λ_m. The number of ordered pairs in a set is g_m. The pair separation is $\sigma_m R_0$. Also tabulated are $\cos\theta_m$, where θ_m is the angle subtended by the pair, and the asymptotic values of the weights D_m from Eq. (2.43) and D'_m from Eq. (2.48).

m	g_m	σ_m	$\cos\theta_m$	$D_m(\infty)$	$D'_m(\infty)$
0	12	$\sqrt{0}$	1	1.382200	2.248640
1	48	$\sqrt{1}$	1/2	0.345550	0.562160
2	24	$\sqrt{2}$	0	0.320796	0.438994
3	48	$\sqrt{3}$	−1/2	0.407861	0.546642
4	12	$\sqrt{4}$	−1	0.448817	0.627726

and subtending the same angle θ_m with the relaxing atom α. For a pair of neighbors β and δ in set Λ_m, the angle is given by

$$\cos\theta_m=\mathbf{n}_\beta\cdot\mathbf{n}_\delta. \tag{2.35}$$

The partitioning is summarized in Table I.

For pairs (β,δ) in the same set Λ_m, the angular integrals (2.32) will be identical, and we designate them by

$$J_m(u)=1+j_0(u\sigma_m\phi_D)-2j_0(u\phi_D), \tag{2.36}$$

where the phonon momentum u, in units of the Debye momentum $\hbar k_D$, is

$$u=k/k_D=E/E_D, \tag{2.37}$$

and

$$\phi_D=k_D R_0=(6\pi^2\sqrt{2})^{1/3} \tag{2.38}$$

is the phase advance over the nearest-neighbor distance R_0 for a phonon with the Debye wave number k_D.

If we average Eq. (2.31) over phonon occupation numbers in thermal equilibrium, the results are the Bose-Einstein distributions

$$\langle n_{\mathbf{k}_a j_a}\rangle=\frac{1}{e^{E_a/k_BT}-1}\quad\text{and}\quad\langle n_{\mathbf{k}_e j_e}+1\rangle=\frac{e^{E_e/k_BT}}{e^{E_e/k_BT}-1}. \tag{2.39}$$

Since polycrystalline samples have been used in most, if not all, magnetic resonance experiments on ^{129}Xe in the solid phase of the xenon, we should average Eq. (2.31) over all possible orientations of the xenon crystal. As a result of this averaging, which we denote by angle brackets $\langle\cdots\rangle$, the partial sums of Eq. (2.31) over pairs of nearest neighbors in the set Λ_m can be written as

$$\left\langle\mathbf{x}_+\cdot\left[\sum_{(\beta\delta)\in\Lambda_m}\sum_{j_e j_a}\mathbf{w}_\beta\mathbf{w}_\delta\right]\cdot\mathbf{x}_-\right\rangle=g_m\sum_l c_l(\epsilon_0)P_l(\cos\theta_m), \tag{2.40}$$

where P_l denotes the Legendre polynomial of order l. The nonzero coefficients $c_l(\epsilon_0)$ are

$$c_0(\epsilon_0)=4+\frac{8}{3}\epsilon_0+\frac{4}{9}\epsilon_0^2,$$

$$c_2(\epsilon_0)=\frac{2}{9}\epsilon_0^2. \tag{2.41}$$

The derivation of Eqs. (2.40) and (2.41) is outlined in the Appendix.

Finally, we introduce $T^*=T/T_D$, the ratio of the crystal temperature to the Debye temperature. Then Eq. (2.31) reduces to Eq. (1.5). The ''freezing out'' of phonons at temperatures below the Debye temperature ($T^*\lesssim 1$) is described by the function

$$\eta^S(\epsilon_0,T^*)=\sum_{lm} g_m c_l(\epsilon_0) P_l(\cos\theta_m) D_m(T^*), \tag{2.42}$$

with the coefficients $D_m(T^*)$—denoted by the same symbol as the analogous coefficients introduced by van Kranendonk[7]—defined by

$$D_m(T^*)=\frac{1}{T^{*2}}\int_0^1 du\, u^4 \frac{e^{u/T^*}}{(e^{u/T^*}-1)^2} J_m^2(u). \tag{2.43}$$

The coupling efficiency $\eta^S(\epsilon_0,T^*)$ is shown as a function of T^* in Fig. 1(a) for representative parameters of solid xenon. For high temperatures ($T^*\gg 1$), the weights $D_m(T^*)$ and hence $\eta^S(\epsilon_0,T^*)$ approach constant values (the asymptotic values of $D_m(T^*)$ are given in Table I), and the relaxation rate (1.5) has a T^{*2} dependence. For temperatures $T^*\ll 0.01$, one can readily show that $\eta^S(\epsilon_0,T^*)$ is proportional to T^{*5}. However, the predicted relaxation times for ^{129}Xe in solid xenon are so long ($T_1^S\gtrsim 10^8$ years for $T^*\lesssim 0.01$) that the low-temperature limiting expressions are of no practical significance.

As described in more detail in Sec. III, measurements of the chemical shift of the nuclear magnetic resonance frequencies of frozen and gaseous ^{129}Xe can be used with Eq. (1.9) to infer that $c_{K0}/h=-27$ Hz for frozen xenon. In Sec. IV, we estimate $\epsilon_0=-11.8$. Evaluating Eq. (1.5) with these values of c_{K0}/h and ϵ_0, and for a xenon crystal temperature T equal to the Debye temperature $T_D=55$ K, we find that the predicted longitudinal relaxation time is $T_1^S=3.9$ h, very close to the observed relaxation time of 3.4 h for $T=51$ K and $B_0\approx 1000$ G.

We follow a nearly identical treatment to that above for the paramagnetic antishielding contribution to the relaxation rate, using primes to distinguish symbols for the paramagnetic antishielding calculations from their spin-rotation counterparts. Using Eqs. (2.19), (2.23), (2.30), (2.32), (2.36), and (2.39), we find in analogy to Eq. (2.31)

$$\frac{1}{T_1^P}=\frac{9\pi c_{K0}^2}{4\hbar^2\omega_D}\sum_m \left\langle \mathbf{x}_+\cdot\left[\sum_{(\beta\delta)\in\Lambda_m}\sum_{j_e j_a} \mathbf{w}'_\beta \mathbf{w}'_\delta\right]\cdot\mathbf{x}_-\right\rangle \times\int_0^1 du\, u^2 \frac{e^{u/T^*}}{(e^{u/T^*}-1)^2} J_m^2(u). \tag{2.44}$$

The angle brackets in Eq. (2.44) indicate an average over all orientations of the xenon crystal, as is appropriate for a polycrystalline sample. In analogy to Eq. (2.40) we find

$$\left\langle \mathbf{x}_+\cdot\left[\sum_{(\beta\delta)\in\Lambda_m}\sum_{j_e j_a} \mathbf{w}'_\beta \mathbf{w}'_\delta\right]\cdot\mathbf{x}_-\right\rangle = g_m\left(\frac{\omega_0}{\omega_D}\right)^2\sum_l c'_l(\epsilon_0) P_l(\cos\theta_m), \tag{2.45}$$

with nonzero coefficients

$$c'_0(\epsilon_0)=\left(1+\frac{3\epsilon_0}{5}+\frac{\epsilon_0^2}{15}\right)^2,$$

$$c'_2(\epsilon_0)=\frac{11\epsilon_0^2(\epsilon_0+6)^2}{630},$$

$$c'_4(\epsilon_0)=\frac{2\epsilon_0^2(\epsilon_0-1)^2}{175}. \tag{2.46}$$

The derivation of Eqs. (2.45) and (2.46) is outlined in the Appendix.

Substituting Eq. (2.45) into Eq. (2.44), we obtain Eq. (1.6), where we have introduced, as in Eq. (2.42), the phonon freeze-out function

$$\eta^P(\epsilon_0,T^*)=\sum_{lm} g_m c'_l(\epsilon_0) P_l(\cos\theta_m) D'_m(T^*), \tag{2.47}$$

with the coefficients

$$D'_m(T^*)=\frac{1}{T^{*2}}\int_0^1 du\, u^2 \frac{e^{u/T^*}}{(e^{u/T^*}-1)^2} J_m^2(u). \tag{2.48}$$

The asymptotic values of $D'_m(T^*)$ are listed in Table I.

For high temperatures $T^*\gg 1$, the ratio of the paramagnetic antishielding relaxation rate (1.6) to that from spin rotation (1.5) is given by

$$\frac{1/T_1^P}{1/T_1^S}\sim\left(\frac{\omega_0}{\omega_D}\right)^2\frac{\eta^P(\epsilon_0,\infty)}{\eta^S(\epsilon_0,\infty)}=3.30\left(\frac{\omega_0}{\omega_D}\right)^2=3.30\left(\frac{B_0}{B_D}\right)^2, \tag{2.49}$$

where $B_D=82$ T is the field for which $\omega_0=\omega_D$, and we have used the value $\epsilon_0=-11.8$ derived in Sec. IV. As shown in Fig. 1(b), the ratio of efficiencies in Eq. (2.49) is only weakly dependent on temperature for $T^*\gtrsim 0.4$ ($T\gtrsim 20$ K): it is only 3.50 at $T^*=0.4$ ($T=22$ K), but 7.39 at $T^*=0.1$ ($T=5.5$ K).

Raman scattering through the spin-rotation interaction and through the paramagnetic antishielding interaction are relaxation mechanisms acting simultaneously and independently, since their cross terms do not contribute to the relaxation. The total relaxation rate due to Raman scattering is thus

$$\frac{1}{T_1}=\frac{1}{T_1^S}+\frac{1}{T_1^P}. \tag{2.50}$$

We conclude this section by showing that the relaxation rates due to one-phonon scattering are completely negligible compared to the rates due to Raman scattering. Using Eq. (2.16) to calculate the high-temperature relaxation rate due one-phonon scattering, we find

$$\frac{1}{T_1^S}\sim\lambda\frac{MR_0^2\mu_K^4}{T_D^5}\left(\frac{c_{K0}}{h}\right)^2 T B_0^4, \tag{2.51}$$

where the coefficient is

$$\lambda = \frac{2^{10}\pi^4\phi_D^2}{hk_B^4} = 7.94\times 10^{95}\ \text{erg}^{-5}\ \text{s}^{-1}\ \text{K}^4. \quad (2.52)$$

Here μ_K is the magnetic moment of the spin-1/2 nucleus and B_0 is the magnitude of the applied magnetic field. Equation (2.51) can be derived by methods similar to, but simpler than, those sketched above. Substituting values of physical parameters[8] appropriate for the relaxation of solid ^{129}Xe: $M=2.18\times10^{-22}$ g, $R_0=4.4\times10^{-8}$ cm, $\mu_K=-3.90\times10^{-24}$ erg/G, $T=T_D=55$ K, $c_{K0}/h=-27$ Hz, and $B_0=10$ kG, we find $T_1^S\sim5.2\times10^{14}$ years. Even for $B_0=B_D=820$ kG, $T_1^S\sim1.2\times10^7$ years.

Using Eq. (2.17) to calculate the one-phonon scattering, we find

$$\frac{1}{T_1^P}\sim\lambda'\frac{MR_0^2\mu_K^2\mu_B^2}{T_D^5}\left(\frac{c_{K0}}{h}\right)^2 TB_0^4(\epsilon_0^2+8\epsilon_0+20), \quad (2.53)$$

with

$$\lambda' = \frac{12\pi^4\phi_D^2}{hk_B^4} = 9.29\times10^{93}\ \text{erg}^{-5}\ \text{s}^{-1}\ \text{K}^4. \quad (2.54)$$

The rate (2.53) from fluctuations in the paramagnetic antishielding is bigger than the rate (2.51) due to the spin-rotation interaction by a factor $\sim(\mu_B/\mu_K)^2\sim10^7$. Using the above parameters with the Bohr magneton $\mu_B=9.27\times10^{-21}$ erg/G and $\epsilon_0=-11.8$, we find $T_1^P\sim1.2\times10^8$ years for $B_0=10$ kG, and 2.7 years for $B_0=B_D$, so the predicted rate from Eq. (2.53) is still negligible. The cross term between the matrix elements for the two single-phonon interactions again vanishes.

III. SPIN-ROTATION COUPLING AND THE CHEMICAL SHIFT

In the next two sections we analyze two closely related phenomena: the spin-rotation interaction between colliding Xe atoms, and the paramagnetic antishielding of an externally applied magnetic field at a Xe nucleus caused by the electrons of neighboring atoms. Much of the fundamental physics of these phenomena was discussed by Ramsey.[2] Torrey[5] showed how to use the connection between the chemical shift and the spin-rotation interaction to account for the relaxation of ^{129}Xe in dense Xe gas. In this section we discuss aspects of the physics that are largely independent of models of the electronic structure. In Sec. IV we outline a simple way to estimate the spin-rotation coupling coefficients.

Consider the following two situations:

(1) A stationary crystal in an externally applied magnetic field $\mathbf{B}_0$. Associated with this field is the Larmor frequency

$$\boldsymbol{\omega}_0 = \frac{e}{2mc}\mathbf{B}_0, \quad (3.1)$$

where $-e$ is the electron charge and m the electron mass. We choose a gauge in which the spatially uniform, externally applied magnetic field $\mathbf{B}_0=\nabla\times\mathbf{A}_0$ is described by the vector potential

$$\mathbf{A}_0 = \frac{1}{2}\mathbf{B}_0\times\mathbf{r}, \quad (3.2)$$

and we denote the ground-state many-electron wave function at time t by $\Psi_1=\Psi_1(\mathbf{r}_1,\mathbf{r}_2,\ldots,t)$, where the location of the first electron is $\mathbf{r}_1$, the location of the second is $\mathbf{r}_2$, etc.

(2) A rotating crystal with no externally applied magnetic field. The crystal is rotating with the angular velocity $-\boldsymbol{\omega}_0$, with $\boldsymbol{\omega}_0$ defined by Eq. (3.1). We denote the ground-state many-electron wave function for this case by $\Psi_2=\Psi_2(\mathbf{r}_1,\mathbf{r}_2,\ldots,t)$.

In both of the two cases outlined above, which we denote with a subscript $i=1$ or 2, current densities $\mathbf{J}_i=\mathbf{J}_i(\mathbf{r})$ will be induced at each point $\mathbf{r}$ in the crystal. We ignore any currents coming from the paired electron spins or from the nuclear spins, and we assume that only the *motion* of the electrons and nuclei contributes to $\mathbf{J}_i$. We will also ignore any contributions to the current from thermal vibrations of the crystal (phonons), although an important result of this phonon-free analysis will be used to make a connection between chemical shifts of xenon and phonon-induced, spin-lattice relaxation rates. The current $\mathbf{J}_i$ will generate a magnetic field $\mathbf{B}_i$ at the nucleus of atom α, which we take to be at the origin of a spatial coordinate system. According to the Biot-Savart law the field is

$$\mathbf{B}_i = \int d^3\mathbf{r}\,\frac{\mathbf{r}\times\mathbf{J}_i}{cr^3}. \quad (3.3)$$

The operator for the electron current density at the spatial position $\mathbf{r}$ is

$$\hat{\mathbf{J}}_e = \frac{-e}{2m}\sum_j\,[\,\delta(\mathbf{r}-\mathbf{r}_j)\boldsymbol{\pi}_j+\boldsymbol{\pi}_j\delta(\mathbf{r}-\mathbf{r}_j)\,] = \hat{\mathbf{J}}_p+\hat{\mathbf{J}}_d, \quad (3.4)$$

where the mechanical momentum for the electron j is $\boldsymbol{\pi}_j=\mathbf{p}_j+(e/c)\mathbf{A}_0(\mathbf{r}_j)$, and the canonical momentum is $\mathbf{p}_j=\hbar\nabla_j/i$. The sum in Eq. (3.4) includes each electron j in the crystal. As indicated in Eq. (3.4), $\hat{\mathbf{J}}_e$ is the sum of a paramagnetic part,

$$\hat{\mathbf{J}}_p = \frac{-e}{2m}\sum_j\,[\,\delta(\mathbf{r}-\mathbf{r}_j)\mathbf{p}_j+\mathbf{p}_j\delta(\mathbf{r}-\mathbf{r}_j)\,], \quad (3.5)$$

and a diamagnetic part,

$$\hat{\mathbf{J}}_d = \frac{-e^2}{mc}\sum_j\,\mathbf{A}_0(\mathbf{r}_j)\,\delta(\mathbf{r}-\mathbf{r}_j) = \boldsymbol{\omega}_0\times\mathbf{r}\hat{\rho}_e. \quad (3.6)$$

Here the operator for the electron charge density is

$$\hat{\rho}_e = -e\sum_j\,\delta(\mathbf{r}-\mathbf{r}_j). \quad (3.7)$$

The expressions (3.5) and (3.6) for the paramagnetic and diamagnetic current densities are appropriate for the gauge of Eq. (3.2). The expectation value $\langle\mathbf{J}_e\rangle$ of the total electronic current density (3.4) is gauge invariant.

In the rotating crystal, $\mathbf{A}_0=0$, and there is no diamagnetic contribution to the current density. There is, however, a contribution from the rotating, charged nuclei, given by

$$\mathbf{J}_{n2} = -\boldsymbol{\omega}_0 \times \mathbf{r}\rho_n , \tag{3.8}$$

where $\rho_n = Z\Sigma_\nu \delta(\mathbf{r} - \mathbf{R}_\nu^{(0)})$ is the charge density at $\mathbf{r}$ from Xe nuclei of atomic number $Z = 54$ located at positions $\mathbf{R}_\nu^{(0)}$ in the crystal. The $\mathbf{R}_\nu^{(0)}$ will rotate with the rotating crystal, but they will be time independent for the nonrotating crystal in the magnetic field.

The total current densities for the two cases are

$$\mathbf{J}_1 = \mathbf{J}_{p1} + \mathbf{J}_{d1} = \langle \Psi_1 | \hat{\mathbf{J}}_p | \Psi_1 \rangle + \langle \Psi_1 | \hat{\mathbf{J}}_d | \Psi_1 \rangle,$$

$$\mathbf{J}_2 = \mathbf{J}_{p2} + \mathbf{J}_{n2} = \langle \Psi_2 | \hat{\mathbf{J}}_p | \Psi_2 \rangle + \mathbf{J}_{n2} . \tag{3.9}$$

Substituting Eq. (3.9) into Eq. (3.3), we find that the corresponding magnetic fields at the origin are

$$\mathbf{B}_1 = \mathbf{B}_{p1} + \mathbf{B}_{d1} , \tag{3.10}$$

$$\mathbf{B}_2 = \mathbf{B}_{p2} + \mathbf{B}_{n2} . \tag{3.11}$$

To find the expectation value of the current density operators, we need the ground-state electronic wave functions Ψ_i. In the case of a stationary crystal in an applied magnetic field, the wave function is

$$\Psi_1 = e^{-iE_1 t/\hbar} \Phi_1 , \tag{3.12}$$

where $\Phi_1 = \Phi_1(\mathbf{r}_1, \mathbf{r}_2, \ldots)$ is the lowest-energy solution of the time-independent Schrödinger equation

$$(H^{(0)} + \hbar \boldsymbol{\omega}_0 \cdot \mathbf{L} + V^{(2)} - E_1)\Phi_1 = 0. \tag{3.13}$$

Here $H^{(0)}$ is the Hamiltonian of the stationary crystal with no applied field, $\mathbf{L} = (1/\hbar)\Sigma_j \mathbf{r}_j \times \mathbf{p}_j$ is the total orbital angular momentum of the electrons (in units of $\hbar$), and $V^{(2)} = (m/2)\Sigma_j |\boldsymbol{\omega}_0 \times \mathbf{r}_j|^2$ is the ''diamagnetic potential.''

In the rotating crystal with no magnetic field, the ground-state electronic wave function is[19]

$$\Psi_2 = e^{-iE_2 t/\hbar} e^{i\boldsymbol{\omega}_0 \cdot \mathbf{L} t} \Phi_2 , \tag{3.14}$$

where $\Phi_2 = \Phi_2(\mathbf{r}_1, \mathbf{r}_2, \ldots)$ is the lowest-energy stationary state of the Schrödinger equation[19] in a coordinate system rotating along with the crystal at angular velocity $-\boldsymbol{\omega}_0$,

$$(H^{(0)} + \hbar \boldsymbol{\omega}_0 \cdot \mathbf{L} - E_2)\Phi_2 = 0. \tag{3.15}$$

Equations (3.13) and (3.15) differ only by the diamagnetic potential $V^{(2)}$, which is second order in $\boldsymbol{\omega}_0$. Thus, the ground-state energies E_1 and E_2 are the same to order $\boldsymbol{\omega}_0$, as are the wave functions $\Psi_1(t=0) = \Phi_1$ and $\Psi_2(t=0) = \Phi_2$. Also, the paramagnetic current densities $\mathbf{J}_{p1} = \langle \Psi_1 | \hat{\mathbf{J}}_p | \Psi_1 \rangle$ and $\mathbf{J}_{p2} = \langle \Psi_2 | \hat{\mathbf{J}}_p | \Psi_2 \rangle$ will be the same to order $\boldsymbol{\omega}_0$ at time $t = 0$. For the nonrotating crystal, the currents induced by the applied magnetic field are time independent; in the rotating crystal, the current distribution $\langle \Phi_2 | \hat{\mathbf{J}}_p | \Phi_2 \rangle$ viewed in the rotating frame is time independent, but the current distribution $\langle \Psi_2 | \hat{\mathbf{J}}_p | \Psi_2 \rangle$ seen from the laboratory frame will rotate rigidly with the crystal.

Since the paramagnetic currents at the time $t = 0$ are the same to order $\boldsymbol{\omega}_0$, the paramagnetic contributions to the magnetic fields are equal as well, and we can write the difference of the fields (3.10) and (3.11) at $t = 0$ as

$$\mathbf{B}_3 \equiv \mathbf{B}_1 - \mathbf{B}_2 = \int d^3\mathbf{r} \, \frac{1}{cr^3} \mathbf{r} \times (\boldsymbol{\omega}_0 \times \mathbf{r})(\rho_e + \rho_n). \tag{3.16}$$

This is the field that would be produced at the origin at time $t = 0$ if the charge densities $\rho_e = \langle \Phi_1 | \hat{\rho}_e | \Phi_1 \rangle$ and ρ_n were rotating rigidly forward with angular velocity $\boldsymbol{\omega}_0$. These charge densities, however, are almost exactly the same as those for isolated Xe atoms. The differences are mostly due to the small spillover of the outermost electrons into the cores of neighboring atoms. While this spillover is of great importance to the paramagnetic currents (see Sec. IV), it produces negligible diamagnetism and we ignore its contribution to Eq. (3.16).

The field (3.16) will have contributions from ρ_e but not ρ_n for the central atom α, and it will have contributions from both ρ_e and ρ_n for all other atoms. For the neighboring atoms, the rotation about the origin can be viewed as a combination of linear translation and a rotation about each atom's nucleus. A neutral, translating atom produces no magnetic field outside of its electronic shells. Although the rotation of the electron charge density ρ_e about the nucleus of an atom produces a magnetic dipole field outside of the atom, the dipole fields from the atoms surrounding the central atom α cancel at the origin because of the high symmetry of the fcc lattice. Thus, the only significant contribution to the field $\mathbf{B}_3$ comes from the rotating electron charge density ρ_e of atom α. This contribution is the same as that of the diamagnetic current (3.6) produced when the atom α is isolated and in an externally applied magnetic field $\mathbf{B}_0$. In this case, the total field at the nucleus would be $\mathbf{B}_0 + \mathbf{B}_3 = (1 - \sigma_g)\mathbf{B}_0$, where σ_g is the isotropic chemical shift of xenon gas. We conclude from Eq. (3.16) that

$$\mathbf{B}_1 - \mathbf{B}_2 = -\sigma_g \mathbf{B}_0 = -\frac{2mc\sigma_g}{e}\boldsymbol{\omega}_0 . \tag{3.17}$$

Although the results (3.16) and (3.17) were derived for $t = 0$, they are valid for all times. The field $\mathbf{B}_2$ rotates with the angular velocity $-\boldsymbol{\omega}_0$, but for the polycrystalline samples considered here, the ensemble-averaged value of $\mathbf{B}_2$ will be parallel to $\boldsymbol{\omega}_0$, and the rotation will leave $\mathbf{B}_2$ unchanged.

In the crystal rotating with angular velocity $-\boldsymbol{\omega}_0$, the relative angular momentum $\mathbf{N}_{\beta\alpha}$ between atom α and nearest-neighbor atom β will be given by Eqs. (1.2) and (1.3), with $\boldsymbol{\omega} = -\boldsymbol{\omega}_0$ and the interatomic displacement $\mathbf{R} = \mathbf{R}_{\beta\alpha}^{(0)} = \mathbf{R}_\beta^{(0)}$ from Eq. (2.12). The spin-rotation interaction (1.1) between the nuclear spin $\mathbf{K}$ of atom α and the relative angular momenta $\mathbf{N}_{\beta\alpha}$, summed over all 12 nearest neighbors β, must be the same as the interaction $-\boldsymbol{\mu}_K \cdot \mathbf{B}_2$ of the nuclear moment $\boldsymbol{\mu}_K = (\mu/K)\mathbf{K}$ of atom α with the induced field $\mathbf{B}_2$. Therefore, from Eqs. (1.1) and (1.3),

$$-\frac{\mu_K}{K}\mathbf{K} \cdot \mathbf{B}_2 = \frac{c_{K0}}{\hbar}\mathbf{K} \cdot \left[\sum_\beta \frac{M}{2} (R_\beta^{(0)2}\mathbf{1} - \mathbf{R}_\beta^{(0)}\mathbf{R}_\beta^{(0)}) \right] \cdot (-\boldsymbol{\omega}_0)$$

$$= -\frac{4c_{K0}MR_0^2}{\hbar}\mathbf{K} \cdot \boldsymbol{\omega}_0 , \tag{3.18}$$

where the sum in square brackets is half the moment of inertia of the cube containing atom α and all 12 nearest neigh-

bors β sketched in Fig. 3. Because of the high symmetry of the fcc crystal, the moment of inertia of the cube reduces to the scalar $8MR_0^2$, and Eq. (3.18) implies that

$$\mathbf{B}_2=\frac{4c_{K0}MR_0^2K}{\hbar\mu_K}\boldsymbol{\omega}_0. \tag{3.19}$$

In the stationary crystal, the total field acting at the origin is $\mathbf{B}_0+\mathbf{B}_1=(1-\sigma_c)\mathbf{B}_0$, where σ_c is the isotropic chemical shift of xenon crystals. Thus

$$\mathbf{B}_1=-\sigma_c\mathbf{B}_0=-\frac{2mc\sigma_c}{e}\boldsymbol{\omega}_0. \tag{3.20}$$

Substituting Eqs. (3.20) and (3.19) into Eq. (3.17) we obtain the fundamental relation (1.9).

Raftery *et al.*[9] recently measured the relative chemical shift $\sigma_g-\sigma_c$ between the gas and the solid phases of ^{129}Xe. At $T=77$ K, they determined $\sigma_g-\sigma_c=317\times10^{-6}$. Substituting this result into Eq. (1.9), along with the known parameters[8] for ^{129}Xe, $M=2.18\times10^{-22}$ g, $R_0=4.4$ Å, $\mu_K=-3.90\times10^{-24}$ erg/G, and $K=1/2$, we find

$$\frac{c_{K0}}{h}=-27\ \text{Hz}. \tag{3.21}$$

IV. ESTIMATES OF c_K

Here we discuss a simple theoretical method, based on an orthogonalization procedure introduced by Wu *et al.*,[16] which gives paramagnetic modifications of magnetic shielding coefficients or spin-rotation coupling coefficients which are about as close to experimental observation as those obtained by Ramsey's[2] second-order perturbation theory as applied by Adrian.[17] No sum over intermediate states of perturbation theory is needed, since the method is basically a first-order estimate of c_K by pseudopotential theory. It could be improved by the systematic application of higher-order corrections.[18]

We estimate the magnetic field $\mathbf{B}_2$ of Eq. (3.11) that is produced at the origin when a crystal rotates with angular velocity $-\boldsymbol{\omega}_0$, as discussed in Sec. III. For single-particle electron wave functions (orbitals) we will use the ''tight-binding'' approximation, which should be especially appropriate for solid noble gases. The many-electron wave function Φ_2 of Eq. (3.14) will be a Slater determinant of the single-electron orbitals $\phi_{j\nu}=\phi_{j\nu}(\mathbf{r})$ for an electron at position $\mathbf{r}$ and in the quantum state j localized near the equilibrium position $\mathbf{R}_\nu^{(0)}$ of nucleus ν. We write the orbitals as

$$\phi_{j\nu}=\chi_{j\nu}e^{i\mathbf{q}_\nu\cdot\mathbf{r}}, \tag{4.1}$$

the product of an orbital amplitude $\chi_{j\nu}=\chi_{j\nu}(\mathbf{r})$, and a phase factor $e^{i\mathbf{q}_\nu\cdot\mathbf{r}}$, where

$$\mathbf{q}_\nu=-\frac{m}{\hbar}\boldsymbol{\omega}_0\times\mathbf{R}_\nu^{(0)} \tag{4.2}$$

is the spatial frequency the electron would have if it were moving with the velocity $-\boldsymbol{\omega}_0\times\mathbf{R}_\nu^{(0)}$ of nucleus ν in the rotating crystal.

We want to estimate the magnetic field $\mathbf{B}_2$ of Eq. (3.11) at the origin of the rotating coordinate system where the nucleus α is located. From Eq. (3.5) we see that at time $t=0$, an electron in the orbital $\phi_{j\nu}$ contributes a paramagnetic current density

$$\mathbf{j}_{j\nu}=\frac{-e\hbar}{m}\mathbf{q}_\nu|\chi_{j\nu}|^2+\left[\frac{-e\hbar}{2mi}\chi_{j\nu}^*\boldsymbol{\nabla}\chi_{j\nu}+\text{c.c.}\right]. \tag{4.3}$$

The first term in Eq. (4.3) is the current resulting from translation of the orbital charge density at the velocity $\hbar\mathbf{q}_\nu/m$. When Eq. (4.3) is summed over all orbitals and multiplied by 2 to account for the spin-up and spin-down electrons occupying each orbital, the field at the origin resulting from the first term is very nearly cancelled by the field $\mathbf{B}_{n2}$ from the nuclear current $\mathbf{J}_{n2}$ of Eq. (3.8), as discussed in the previous section. Thus the field at the origin is almost entirely due to the current density $\mathbf{J}_2=\mathbf{J}_2(\mathbf{r})$ given by contributions from the second term of Eq. (4.3),

$$\mathbf{J}_2=\frac{-e\hbar}{mi}\sum_{j\nu}\chi_{j\nu}^*\boldsymbol{\nabla}\chi_{j\nu}+\text{c.c.} \tag{4.4}$$

Substituting Eq. (4.4) into the Biot-Savart Law (3.3), we find for the field at the origin

$$\mathbf{B}_2=\frac{-2e\hbar}{mc}\sum_{j\nu}\int d^3\mathbf{r}\,\chi_{j\nu}^*\frac{\mathbf{l}}{r^3}\chi_{j\nu}, \tag{4.5}$$

where $\mathbf{l}=-i\mathbf{r}\times\boldsymbol{\nabla}$ is the electron orbital angular momentum operator (in units of $\hbar$).

The orbitals $\phi_{j\nu}$ in Eq. (4.1) are solutions to the Schrödinger equation

$$\left[-\frac{\hbar^2}{2m}\nabla^2+v(\mathbf{r})-i\hbar\boldsymbol{\omega}_0\cdot\mathbf{r}\times\boldsymbol{\nabla}-\epsilon_{j\nu}\right]\phi_{j\nu}=0. \tag{4.6}$$

The orbital energy is $\epsilon_{j\nu}$. The effective single-particle potential $v(\mathbf{r})$ has the periodicity of the crystal lattice, but the solutions of Eq. (4.6) are not Bloch functions because of the presence of the nonperiodic potential $-i\hbar\boldsymbol{\omega}_0\cdot\mathbf{r}\times\boldsymbol{\nabla}$, which represents Coriolis and centrifugal forces on the electron. Substituting expressions (4.1) and (4.2) into Eq. (4.6), we see that if the potential v were the same as the potential of a free Xe atom located at $\mathbf{R}_\nu^{(0)}$, the orbital amplitudes $\chi_{j\nu}$ would be identical to the orbitals $\chi_{j\nu}^{(0)}$ of free Xe atoms, to first order in ω_0. The outermost, $5p$ orbitals of the Xe atom are responsible for most of the phenomena under consideration here, and we will write them as

$$\chi_{j\nu}^{(0)}(\mathbf{r})=\chi_{5pk\nu}^{(0)}(\mathbf{r})=\sqrt{\frac{3}{4\pi}}\frac{U_{5p}(s_\nu)}{s_\nu}\mathbf{s}_\nu\cdot\mathbf{x}_k, \tag{4.7}$$

where $\mathbf{x}_k$ $(k=1,2,3)$ is a unit vector along one of the three crystal coordinate axes and the displacement of the electron from the nucleus ν is

$$\mathbf{s}_\nu=\mathbf{r}-\mathbf{R}_\nu^{(0)}. \tag{4.8}$$

Because contributions from the orbitals to the field $\mathbf{B}_2$ in Eq. (4.5) are weighted by $1/r^3$, we need only consider components of the electron wave functions within the core of the central atom α. In principle, we should sum over all electron orbitals of the crystal in Eq. (4.5). However, the spin-paired

electrons in the closed shells of atom α will make negligible contributions to the field. In the tight-binding approximation considered here, the orbital amplitudes for next-nearest and more distant atoms will be too small near the origin to contribute substantially to the sum in Eq. (4.5). Only for an orbital centered on one of the nearest-neighbor atoms β can we expect a substantial contribution to $\mathbf{B}_2$. Such orbitals will ''spill over'' into the core of atom α, where they will have a secondary peak due to the attraction to the nucleus of the atom α. Following Wu *et al.*,[16] we can approximate this penetration of the nearest-neighbor cores by orthogonalizing the orbitals of atom β to the orbitals of atom α. We consider only the overlaps of the $5p$ orbitals, since they will contribute much more to the field $\mathbf{B}_2$ than any others. Near $\mathbf{r}=0$, we can approximate the orbital $\phi_{5pb\beta}$ of atom β by

$$\phi_{5pb\beta} \approx \chi^{(0)}_{5pb\beta} e^{i\mathbf{q}_\beta\cdot\mathbf{r}} - f\sum_a \chi^{(0)}_{5pa\alpha} S_{ab}. \tag{4.9}$$

The elements S_{ab} of the overlap tensor are given by

$$S_{ab} = \int d^3\mathbf{r}\, \chi^{(0)*}_{5pa\alpha} e^{i\mathbf{q}_\beta\cdot\mathbf{r}} \chi^{(0)}_{5pb\beta}, \tag{4.10}$$

The coefficient $f\approx 1$ is an empirical fitting parameter to be determined from measured chemical shifts. Even though the overlap coefficients S_{ab} are small, the second term of Eq. (4.9) is still much larger, within the core of atom α, than the first term, which we will henceforth ignore.

Using Eq. (4.7) and noting that $\mathbf{s}_\alpha = \mathbf{r}$ since $\mathbf{R}^{(0)}_\alpha = 0$, we write Eq. (4.9) as

$$\phi_{5pb\beta} \approx -f\sqrt{\frac{3}{4\pi}}\frac{U_{5p}(r)}{r}\mathbf{r}\cdot\mathbf{S}_b, \tag{4.11}$$

where the overlap vectors are

$$\mathbf{S}_b = \sum_a \mathbf{x}_a S_{ab}. \tag{4.12}$$

Substituting Eq. (4.11) into Eq. (4.5), and noting that near the nucleus α, $\chi_{5pb\beta} \approx \phi_{5pb\beta}$, we find that the contribution from atom β to the field $\mathbf{B}_2$ at the origin is

$$\mathbf{B}_{2\beta} = \frac{2ei\hbar|f|^2}{mc}\left\langle\frac{1}{r^3}\right\rangle \sum_b \mathbf{S}^*_b\times\mathbf{S}_b. \tag{4.13}$$

The radial matrix element is

$$\left\langle\frac{1}{r^3}\right\rangle = \int_0^\infty dr\,\frac{1}{r}U^2_{5p}(r) = 17.78 a_B^{-3}, \tag{4.14}$$

where $a_B = 5.29\times10^{-9}$ cm is the Bohr radius, and the numerical value of Eq. (4.14) was obtained using the exponential-type wave functions of Clementi and Roetti.[20]

The evaluation of the overlap tensor (4.10) is facilitated by using a coordinate system centered between atoms α and β, with the unit vector $\mathbf{x}'_3$ along the interatomic axis and two additional unit vectors, $\mathbf{x}'_1$ and $\mathbf{x}'_2$, completing the orthonormal Cartesian basis. Then the components of the overlap tensor become

$$S'_{ab} = \frac{3}{4\pi}\int d^3\mathbf{r}\, e^{i\mathbf{q}_\beta\cdot\mathbf{r}} U_{5p}(r)U_{5p}(s)\frac{r'_a s'_b}{rs}, \tag{4.15}$$

where $\mathbf{s}=\mathbf{s}_\beta$, $r'_a = \mathbf{x}'_a\cdot\mathbf{r}$, $s'_b = \mathbf{x}'_b\cdot\mathbf{s}$, etc. We may set $\exp(i\mathbf{q}_\beta\cdot\mathbf{r}) = 1 + i\mathbf{q}_\beta\cdot\mathbf{r}$ in Eq. (4.15), since $|\mathbf{q}_\beta\cdot\mathbf{r}| \lesssim 10^{-2}$ for values of $\mathbf{r}$ where the other factors of the integrand are not negligibly small. Most of the elements of the tensor (4.15) vanish by symmetry; the nonvanishing parts are

$$S'_{ab} = S^{(a)}\delta_{ab} + i\frac{q'_1R_0}{2}S^{(1)}\varepsilon_{ab2} - i\frac{q'_2R_0}{2}S^{(1)}\varepsilon_{ab1} + i\frac{q'_3R_0}{2}S^{(a)}\delta_{ab}, \tag{4.16}$$

where ε_{ijk} is the antisymmetric tensor with $\varepsilon_{123}=1$. The overlap of π orbitals is

$$S^{(1)} = S^{(2)} = \frac{3}{8\pi}\int d^3\mathbf{r}\, U_{5p}(r)U_{5p}(s)\frac{r'_1s'_1 + r'_2s'_2}{rs}, \tag{4.17}$$

and the overlap of σ orbitals is

$$S^{(3)} = \frac{3}{4\pi}\int d^3\mathbf{r}\, U_{5p}(r)U_{5p}(s)\frac{r'_3s'_3}{rs}. \tag{4.18}$$

Since $\mathbf{S}_b = \Sigma_{ij}\mathbf{x}'_i S'_{ij}\mathbf{x}'_j\cdot\mathbf{x}_b = \Sigma_j \mathbf{S}'_j(\mathbf{x}'_j\cdot\mathbf{x}_b)$, and since both $\mathbf{x}_b$ and $\mathbf{x}'_j$ are elements of orthonormal bases, we have

$$\sum_b \mathbf{S}^*_b\times\mathbf{S}_b = \sum_b \mathbf{S}'^*_b\times\mathbf{S}'_b = iS^{(1)}(S^{(1)}+S^{(3)})\mathbf{q}_\beta\times\mathbf{R}^{(0)}_{\beta\alpha}, \tag{4.19}$$

and the expression (4.13) for the field at the origin becomes

$$\mathbf{B}_{2\beta} = \mathbf{N}_{\beta\alpha}\frac{4e\hbar}{Mc}|f|^2\left\langle\frac{1}{r^3}\right\rangle S^{(1)}(S^{(1)}+S^{(3)}). \tag{4.20}$$

Here

$$\mathbf{N}_{\beta\alpha} = \frac{M}{2m}\mathbf{R}^{(0)}_{\beta\alpha}\times\mathbf{q}_\beta \tag{4.21}$$

is the sum of the angular momenta of atoms β and α about their center of mass.

The interaction $-\boldsymbol{\mu}_K\cdot\mathbf{B}_{2\beta}$ of the magnetic moment $\boldsymbol{\mu}_K = (\mu_K/K)\mathbf{K}$ of the nucleus of atom α with the field $\mathbf{B}_{2\beta}$ Eq. (4.20) produced by nearest-neighbor atom β must be the same as the spin-rotation interaction (1.1). Equating

$$c_{K0}\mathbf{K}\cdot\mathbf{N}_{\beta\alpha} = -\frac{\mu_K}{K}\mathbf{K}\cdot\mathbf{B}_{2\beta}, \tag{4.22}$$

we obtain our estimate (1.10) for c_{K0}.

Because of the axial symmetry and even parity of the integrands in Eqs. (4.17) and (4.18), the two-center integrals reduce to two-dimensional integrals. For example, the overlap integral for σ orbitals is

$$S^{(3)} = 2\int_0^\infty U_{5p}(r)k_\sigma(r)\,r^2dr = -8.516\exp(-1.181\ \text{Å}^{-1}R), \tag{4.23}$$

where R is the (possibly nonequilibrium) separation between the nuclei. The integrand of Eq. (4.23) contains the factor

$$k_\sigma(r) = -\frac{3}{2}\int_{\theta_0}^{\pi} U_{5p}(s)\cos\psi\cos\theta\sin\theta\, d\theta. \quad (4.24)$$

R, r, and s form a triangle with s subtending the angle θ and r subtending the angle ψ, so

$$s = \sqrt{R^2 + r^2 - 2Rr\cos\theta}, \text{ and } \cos\psi = \frac{R - r\cos\theta}{s}. \quad (4.25)$$

The angle θ_0 is defined by

$$\theta_0 = \begin{cases} 0, & r \leqslant R/2; \\ \cos^{-1} R/2r, & r > R/2. \end{cases} \quad (4.26)$$

The overlap integral for π orbitals is

$$S^{(1)} = 2\int_0^\infty U_{5p}(r)k_\pi(r)\, r^2 dr = 8.457\exp(-1.578\ \text{Å}^{-1}R), \quad (4.27)$$

where

$$k_\pi(r) = \frac{3}{4}\int_{\theta_0}^{\pi}\frac{r}{s}U_{5p}(s)\sin^3\theta\, d\theta. \quad (4.28)$$

The overlap integrals were determined by numerical integration at $R/a_B = 8.28, 8.30, \ldots, 8.36$ using the exponential-type Roothaan wave functions tabulated by Clementi and Roetti.[20] They were very well described in this range by the exponential functions of the internuclear separation R given in Eqs. (4.23) and (4.27). We also found that over the same interval of internuclear separations, the product of overlap integrals needed to evaluate Eq. (1.10) was well described by

$$S^{(1)}(S^{(1)} + S^{(3)}) = -44.52\exp(-2.693\ \text{Å}^{-1}R), \quad (4.29)$$

Substituting into Eq. (1.10) values for the physical constants, a mean xenon mass $M = 2.18\times10^{-22}$ g, ^{129}Xe nuclear spin $K = 1/2$ and nuclear magnetic moment $\mu_K = -3.90\times10^{-24}$ erg/G, and Eq. (4.29) for the product of the overlap integrals, we find

$$\frac{c_K}{h} = -1.966\times10^6|f|^2\exp(-2.693\ \text{Å}^{-1}R)\ \text{Hz}$$
$$= -14.1|f|^2\ \text{Hz at } R = R_0 = 4.4\ \text{Å}. \quad (4.30)$$

To obtain the value $c_{K0}/h = -27$ Hz inferred in Sec. III from the measured chemical shifts of solid and gaseous xenon, we must have $|f| = 1.38$. We would expect[18] to find $f = 1$ in Eq. (4.9) if the spillover of the wave functions from atom β to atom α could be determined by simple orthogonalization of $5p$ wave functions of free xenon atoms. However, we expect fairly substantial modifications of the $5p$ orbitals of xenon atoms in the solid. For example, the 9.16 eV band gap of solid xenon[21] is substantially less than the 12.13 eV first ionization potential of a free xenon atom. The $5p$ orbitals of xenon atoms in the solid must therefore be more extended than those of a free xenon atom. This greater extension would lead to a larger overlap integral and larger values of $|f|$.

We may also use Eq. (4.30) with Eq. (1.7) to estimate

$$\epsilon = -2.693\ \text{Å}^{-1}R, \quad (4.31)$$

and thus,

$$\epsilon_0 = \epsilon(4.4\ \text{Å}) = -11.8. \quad (4.32)$$

Adrian[17] calculated that $\epsilon/R = -2.506\ \text{Å}^{-1}$, which yields $\epsilon_0 = -11.0$ for $R_0 = 4.4$ Å and agrees with our result (4.32) to within 7%. As discussed by Lurie *et al.*,[22] the experimental data on the temperature dependence of the chemical shift in solid ^{129}Xe are not accurate enough to determine ϵ_0 to better than about 8%.

We can use Eqs. (4.21), (4.2), and (3.1) to write Eq. (4.20) in terms of $\mathbf{B}_0$,

$$\mathbf{B}_{2\beta} = \frac{e^2}{mc^2}|f|^2\left\langle\frac{1}{r^3}\right\rangle S^{(1)}(S^{(1)} + S^{(3)})(\mathbf{R}_\beta^{(0)}\mathbf{R}_\beta^{(0)} - R_0^2\mathbf{1})\cdot\mathbf{B}_0. \quad (4.33)$$

From Eqs. (3.17) and (3.20) we see that for the total field at the origin, $\mathbf{B}_2 = \Sigma_\beta\mathbf{B}_{2\beta}$, we have very nearly

$$\mathbf{B}_2 = \mathbf{B}_1 + \sigma_g\mathbf{B}_0 = -\boldsymbol{\sigma}_p\cdot\mathbf{B}_0, \quad (4.34)$$

a result that is essentially independent of any microscopic model of the electronic structure, as shown in Sec. III. Thus, in solid Xe, $\mathbf{B_1} = -\boldsymbol{\sigma}_c\cdot\mathbf{B}_0$, with the shielding tensor $\boldsymbol{\sigma}_c = \sigma_g\mathbf{1} + \boldsymbol{\sigma}_p$, the sum of the isotropic shielding coefficient σ_g for xenon gas and the paramagnetic antishielding tensor $\boldsymbol{\sigma}_p$ due to neighboring Xe atoms. Using Eqs. (4.34) and (4.33) we find that a Xe atom displaced a distance $\mathbf{R}$ from the shielded nucleus contributes a paramagnetic antishielding tensor

$$\boldsymbol{\sigma}_p = \frac{e^2}{mc^2}|f|^2\left\langle\frac{1}{r^3}\right\rangle S^{(1)}(S^{(1)} + S^{(3)})(R^2\mathbf{1} - \mathbf{RR}). \quad (4.35)$$

The zz component of the tensor is

$$\sigma_{p;zz} = \frac{e^2R^2}{mc^2}|f|^2\left\langle\frac{1}{r^3}\right\rangle S^{(1)}(S^{(1)} + S^{(3)})\sin^2\theta, \quad (4.36)$$

where $\mathbf{R}\cdot\mathbf{x}_3/R = \cos\theta$.

The only previous estimate of paramagnetic contributions to the shielding of pairs of xenon atoms seems to be a perturbation calculation by Adrian,[17] who derives an estimate

$$\sigma_{p;zz} = \frac{16\mu_B^2}{\Delta E}\left\langle\frac{1}{r^3}\right\rangle(S^{(1)} - S^{(3)})^2\sin^2\theta \quad (4.37)$$

for the paramagnetic shielding coefficient σ. In Adrian's notation,[17] the Bohr magneton μ_B was denoted by β and the overlap integrals $S^{(1)}$ and $S^{(3)}$ were denoted by $S_{\pi\pi}$ and $-S_{\sigma\sigma}$, respectively. Adrian chose a mean excitation energy $\Delta E = -9.6$ eV to permit him to sum the perturbation series by closure. Adrian's estimate (4.37) gives the correct sign for the observed pressure-dependent shift of the diamagnetic shielding, but only about 66% of the magnitude.[22]

V. EXPERIMENTS

We have carried out experiments[10] on ^{129}Xe nuclear spin relaxation in solid Xe to determine how much of the measured relaxation might be due to the Raman scattering of phonons discussed above. We used samples for which the value of the nuclear spin polarization had been increased through spin-exchange optical pumping to many orders of magnitude above the thermal equilibrium value.[11,23] This made it possible to study the relaxation of the spin polarization over several e foldings and over a large range of temperatures and applied magnetic fields.

The sample cells used for these measurements were pyrex glass cylinders filled with a few milligrams of Rb metal that had been distilled to reduce impurity contamination. The Xe gas used to fill the cells either had the naturally occurring isotopic mixture, with 26.4% ^{129}Xe, or was from two batches that had been isotopically enriched, one to 72.9% and the other to 80.8% ^{129}Xe. After the alkali metal and gas had been loaded into the cell, it was detached from the gas-filling manifold by fusing the glass fill tube with a hand torch. This left a small ''tip,'' several mm in length, which served later to contain the frozen xenon. In addition to xenon gas, some of the cells were also filled with 80 to 100 torr of N_2 gas to quench excited Rb atoms and prevent reradiated resonance light from depolarizing the spins of the Rb atoms. For applied fields above about 1000 G, the nuclear spin-relaxation time T_1 did not depend on the presence of N_2 in the cell. For smaller applied fields, however, the relaxation rates did depend on the amount of N_2 in the cell. As we discuss below, this was probably due to the dependence of the grain size of the polycrystalline frozen xenon on the amount of N_2 gas in the cell.

During optical pumping, a simple oven was used to maintain the cells at a temperature of about 90 °C, and a longitudinal magnetic field of a few gauss ensured that small ambient magnetic fields caused no spin depolarization. A large electron spin polarization of the Rb atoms was maintained in the cells by laser optical pumping with 3 to 5 W from a Ti:sapphire laser at the 7947 Å Rb D_1 line. Spin-exchange collisions between Xe atoms and the polarized Rb atoms transferred spin angular momentum from the Rb electrons to the nuclei of ^{129}Xe atoms. In about 1/2 hour the ^{129}Xe nuclei reached a saturated polarization $P_0 \simeq 0.15$, which was adequate for subsequent studies of spin relaxation.

After the nuclear spin polarization had saturated, the sample cells were moved to a separate apparatus where liquid nitrogen was used to freeze the polarized ^{129}Xe gas into the tip of the cell. The tip with the frozen xenon was placed in a coil, 1/4 inch in diameter and tuned to resonate at 2.1 MHz. The coil and sample cell were placed inside a flowing He gas cryostat, where the sample could be held at any desired temperature between 4.2 and 77 K, or in a flowing N_2 gas cryostat for temperatures between 77 K and room temperature. The coil with input and output coupling capacitors constituted one branch of an Anderson-type LR balanced twin-T bridge circuit.[24] A Hewlett-Packard signal generator (HP 3325A) served as a radio frequency (rf) source, and the signal across the balanced bridge was amplified by a Princeton Applied Research preamplifier (PAR 115) and detected using a lock-in amplifier (PAR 5202). The cryostat containing the sample and the coil was situated between a pair of Helmholtz coils, 75 cm in diameter, which provided a static field perpendicular to the axis of the resonator coil. The uniformity of the static field was determined to be better than one part in 10^5 over the sample volume (several mm^3). The nuclear spin polarization was measured by detecting the nuclear magnetic induction signal across the coil in the static field $B_{\mathrm{Xe}} = \omega_{\mathrm{Xe}}/\gamma_{\mathrm{Xe}} = 1800$ G, the resonant field for ^{129}Xe at $\omega_{\mathrm{Xe}}/(2\pi) = 2.1$ MHz. Here γ_{Xe} is the ^{129}Xe gyromagnetic ratio. We let the ^{129}Xe relax in the fixed static field B_0, which could be set anywhere from a few gauss to about 2000 G. We sampled the polarization five or six times during the relaxation by briefly changing the field to B_{Xe}. With this scheme, we could only measure relaxation times long compared with the time required to change the field to and from B_{Xe}.

The nuclear magnetic induction signal was created by applying a small rf magnetic field $2B_1 \cos(\omega_0 t)$ to the coil and sweeping the static magnetic field B_0 rapidly through B_{Xe}. The field sweep rate $\dot{\Delta} = \gamma_{\mathrm{Xe}} dB_0/dt$ and the Rabi frequency $\omega_1 = \gamma_{\mathrm{Xe}} B_1$ were adjusted so that the polarization loss during the sweep across the resonance was very small. For a sweep rate $\dot{\Delta} \gg \omega_1^2$ but small compared to the second moment of the absorption line shape for the nuclear spins in the solid, the fractional loss[25] of polarization is $\Delta P/P \approx \pi \omega_1^2/\dot{\Delta}$. Detection losses were reduced to less than 1% by reducing the rf field strength or by increasing the sweep rate. The sample temperature was held constant in the cryostat during the entire decay, which could be a week or more at low temperatures and large magnetic fields. With this detection method, any decrease in signal between successive samplings of the spin polarization was due to spin-lattice relaxation.

Our experiments showed that for sufficiently large magnetic fields $B_0 \gtrsim 1000$ G, and for temperatures $T \geqslant 20$ K, the measured ^{129}Xe polarization P was well described by an exponential decay $P = P_0 \exp(-t/T_1)$ with a single time constant T_1. Furthermore, in this regime the relaxation times T_1 were independent of magnetic field (up to our maximum field of ~ 2000 G), isotopic composition of the Xe, and the presence of any other gas, e.g., N_2, He, or Kr. The high-field relaxation rates for 20 K $< T <$ 120 K are shown in Fig. 2. Also shown is our prediction (1.5) for the relaxation rate due to Raman scattering via the spin-rotation interaction, using $c_{K0}/h = -27$ Hz from Eq. (3.21) and $\epsilon_0 = -11.8$ from Eq. (4.32). The good agreement between experimental and theoretical relaxation rates strongly suggests that the spin-rotation interaction (1.1) dominates the relaxation of solid ^{129}Xe in this regime. For higher temperatures $T > 120$ K, the relaxation becomes dominated by vacancy diffusion.[8,13]

For $T \gtrsim 20$ K and fields $B_0 \sim 1000$ G, Eq. (2.49) implies that the relaxation rate due to the paramagnetic antishielding is smaller than that due to the spin rotation interaction by a factor $\sim (B_0/B_D)^2 \sim 10^{-6}$. However, at the largest currently available magnetic fields (~ 25 T) fluctuations in the paramagnetic antishielding should contribute about 25% of the total relaxation rate.

For $T \lesssim 20$ K or for $B_0 \lesssim 1000$ G, we have found that Raman scattering is insufficient to account for the observed ^{129}Xe relaxation rate, so other mechanisms must be important. A thorough discussion of these other relaxation mecha-

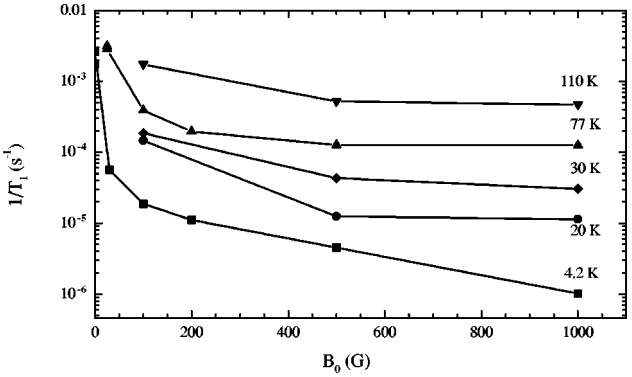

FIG. 4. Dependence on magnetic field of the longitudinal relaxation rate $1/T_1$ of ^{129}Xe in frozen xenon at various temperatures. The data at 110 K were taken with a cell sealed off at a temperature of 25 °C, when it contained 600 Torr of xenon, isotopically enriched to 72.9% ^{129}Xe, and 100 Torr of N_2 gas. The data for all other temperatures were taken with a sample cell filled with 2060 Torr cm^3 of xenon (at 25 °C), isotopically enriched to 80.8% ^{129}Xe with only 3.4% ^{131}Xe, and no other gases. The cell volume was about 3.2 cm^3. The faster relaxation rates at low magnetic fields are due to mechanisms other than Raman scattering of phonons. The solid lines are to guide the eye.

nisms is beyond the scope of this paper, but more details can be found in Refs. 10–12. We present here only a survey of the evidence for one probable mechanism, cross relaxation to ^{131}Xe in the solid.

As shown in Fig. 4, the relaxation rate of ^{129}Xe in the solid has a strong dependence on magnetic field for $B_0 \lesssim 1000$ G. At these lower fields, the coupling of the electric quadrupole moment of the spin-3/2 ^{131}Xe nuclei to electric-field gradients near crystal grain boundaries can bring the ^{131}Xe sublevel energy splittings close to resonance with the ^{129}Xe, allowing for rapid cross relaxation. Because of the short relaxation time of ^{131}Xe, however, the polarization transferred to the ^{131}Xe is rapidly lost, which makes cross relaxation to ^{131}Xe an effective relaxation mechanism for ^{129}Xe.[10–12] This interpretation is supported by the data shown in Fig. 5 of the time dependence of the polarization for four different cells at $B_0 = 1000$ G and $T = 4.2$ K. Cell (a), with only 3.4% ^{131}Xe, had significantly slower relaxation than cell (b) containing natural Xe with 21.2% ^{131}Xe. The Xe in cell (d), which contained Kr buffer gas, was found to freeze much more slowly than in cell (c) with He buffer gas, suggesting that the grain sizes of the polycrystalline ice in cell (d) were larger than in cell (c). From the slower relaxation rate exhibited by cell (d), coupled with the nonexponential decay shown by all four cells and the dependence on ^{131}Xe concentration, we conclude that ^{129}Xe spin diffusion to the grain boundaries, where the ^{129}Xe cross relaxes to ^{131}Xe, plays an important role in the relaxation at low temperatures and low fields. Related studies at 4.2 K have been reported by TonThat *et al.*[12]

ACKNOWLEDGMENTS

This work was supported by the U. S. Air Force Office of Scientific Research under Grant No. F49620-92-J-0211.

APPENDIX: SET AVERAGES

We can use Eq. (2.26) to sum the dyads $\mathbf{w}_\beta \mathbf{w}_\delta$ of Eq. (2.40) over all phonon polarization states to find

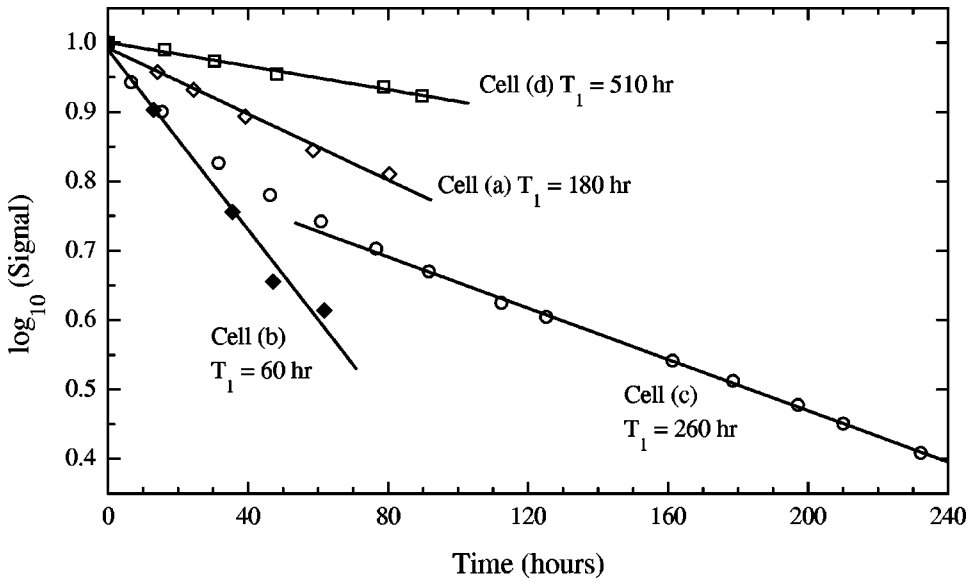

FIG. 5. Experimentally observed nuclear-spin polarization of ^{129}Xe as a function of time at a temperature $T = 4.2$ K and at an applied field $B_0 = 1000$ G. (a) The cell was filled at 25 °C with 600 Torr of xenon gas, isotopically enriched to 80.8% ^{129}Xe with only 3.4% ^{131}Xe. (b) The cell was filled at 25 °C with 600 Torr of xenon gas of natural isotopic composition, 26.4% ^{129}Xe and 21.2% ^{131}Xe. (c) The cell was filled at 25 °C with xenon gas, enriched as in (a) and at a partial pressure of 600 Torr; in addition the cell was filled with helium gas at a partial pressure of 2600 Torr. (d) The cell was filled at 25 °C with xenon gas, enriched as in (a) and at a partial pressure of 300 Torr; in addition the cell was filled with krypton gas at a partial pressure of 300 Torr. The pronounced nonexponential decay of the polarization in cell (c) is probably a consequence of spin diffusion to grain boundaries, where polarization can be transferred from ^{129}Xe to rapidly relaxing ^{131}Xe. The listed values of T_1 correspond to the straight-line fits. Raman scattering of phonons makes a negligible contribution to the low-temperature relaxation seen here.

$$\sum_{j_e j_a} \mathbf{w}_\beta \mathbf{w}_\delta = \mathbf{2} + \epsilon_0[\mathbf{2} - \mathbf{n}_\beta\mathbf{n}_\beta - \mathbf{n}_\delta\mathbf{n}_\delta] + \frac{1}{2}\epsilon_0^2[(\mathbf{n}_\beta\cdot\mathbf{n}_\delta)^2\mathbf{1} - (\mathbf{n}_\beta\cdot\mathbf{n}_\delta)\mathbf{n}_\beta\mathbf{n}_\delta + (\mathbf{n}_\beta\times\mathbf{n}_\delta)(\mathbf{n}_\beta\times\mathbf{n}_\delta)]. \quad \text{(A1)}$$

The bold numerals in Eq. (A1) denote the corresponding multiple of the unit dyadic, for example, $\mathbf{2} = 2(\mathbf{xx} + \mathbf{yy} + \mathbf{zz})$.

We assume the xenon ice is polycrystalline, with the individual crystallites so small that spin diffusion ensures uniform polarization throughout the sample. Then expression (A1) should be averaged over all orientations of the xenon crystal. Let a rigid-body rotation $R = R(\phi, \theta, \psi)$ rotate the crystal about the central nucleus α from the reference position of Fig. 3 to an orientation specified by the Euler angles (ϕ, θ, ψ). Then the unit vector $\mathbf{n}_\beta$ to the nearest-neighbor β is rotated to the new unit vector

$$R\mathbf{n}_\beta = R\sum_q (-1)^q \boldsymbol{\xi}_q n_{\beta;-q} = \sum_{pq} (-1)^q \boldsymbol{\xi}_p D^1_{pq} n_{\beta;-q}. \quad \text{(A2)}$$

Here $D^1_{pq} = D^1_{pq}(\phi, \theta, \psi)$ is a Wigner D function, an irreducible representation of the full rotation group, and the spherical unit vectors are

$$\boldsymbol{\xi}_1 = -\frac{\mathbf{x}_+}{\sqrt{2}} = \frac{\mathbf{x} + i\mathbf{y}}{-\sqrt{2}}, \quad \boldsymbol{\xi}_0 = \mathbf{z}, \quad \boldsymbol{\xi}_{-1} = \frac{\mathbf{x}_-}{\sqrt{2}} = \frac{\mathbf{x} - i\mathbf{y}}{\sqrt{2}}. \quad \text{(A3)}$$

We define the orientational average for a quantity $f = f(\phi, \theta, \psi)$ that depends on the crystal orientation by

$$\langle f \rangle = \frac{1}{8\pi^2}\int f\, d\phi \sin\theta\, d\theta\, d\psi. \quad \text{(A4)}$$

The orientational average of the dyadic (A1) will be denoted by

$$\mathsf{W}_m \equiv \left\langle \sum_{j_e j_a} \mathbf{w}_\beta \mathbf{w}_\delta \right\rangle. \quad \text{(A5)}$$

The averaged dyadic (A5) is the same for any pair $(\beta\delta)$ in the set Λ_m, so the orientationally averaged partial sum (2.40) becomes

$$\left\langle \mathbf{x}_+ \cdot \left[\sum_{(\beta\delta)\in\Lambda_m} \sum_{j_e j_a} \mathbf{w}_\beta \mathbf{w}_\delta \right] \cdot \mathbf{x}_- \right\rangle = g_m \mathbf{x}_+ \cdot \mathsf{W}_m \cdot \mathbf{x}_-. \quad \text{(A6)}$$

Using the orthogonality properties of the Wigner D functions to average the dyad components of Eq. (A1), and recalling that $\mathbf{n}_\beta \cdot \mathbf{n}_\delta = \cos\theta_m$, we find

$$\langle \mathbf{n}_\beta \mathbf{n}_\delta \rangle = \frac{\mathbf{1}}{3}\mathbf{n}_\beta\cdot\mathbf{n}_\delta = \frac{\mathbf{1}}{3}\cos\theta_m. \quad \text{(A7)}$$

A special case of Eq. (A7) is

$$\langle \mathbf{n}_\beta \mathbf{n}_\beta \rangle = \langle \mathbf{n}_\delta \mathbf{n}_\delta \rangle = \frac{\mathbf{1}}{3}. \quad \text{(A8)}$$

By similar arguments, we can show that

$$\langle (\mathbf{n}_\beta\times\mathbf{n}_\delta)(\mathbf{n}_\beta\times\mathbf{n}_\delta) \rangle = \frac{\mathbf{1}}{3}\sin^2\theta_m. \quad \text{(A9)}$$

Substituting Eqs. (A1), (A7), (A8), and (A9) into Eq. (A5) we find

$$\mathsf{W}_m \equiv \left\langle \sum_{j_e j_a} \mathbf{w}_\beta \mathbf{w}_\delta \right\rangle = \left(2 + \frac{4\epsilon_0}{3} + \frac{2\epsilon_0^2}{9} + \frac{\epsilon_0^2 P_2}{9} \right)\mathbf{1}, \quad \text{(A10)}$$

where $P_2 = P_2(\cos\theta_m) = (3\cos^2\theta_m - 1)/2$ is the Legendre polynomial of order 2. Noting that $\mathbf{x}_+ \cdot \mathbf{1} \cdot \mathbf{x}_- = 2$, we find from (A10) that

$$\mathbf{x}_+ \cdot \mathsf{W}_m \cdot \mathbf{x}_- = \left(4 + \frac{8\epsilon_0}{3} + \frac{4\epsilon_0^2}{9} \right) + \frac{2\epsilon_0^2}{9} P_2 = \sum_l c_l(\epsilon_0) P_l. \quad \text{(A11)}$$

Equation (A11), together with Eq. (A6), completes the proof of Eqs. (2.40) and (2.41).

We now turn to the more complicated relaxation produced by the fluctuations in the paramagnetic antishielding. Using Eq. (2.29) to sum the dyads of Eq. (2.44) over the phonon polarization vectors, we find

$$\begin{aligned}\sum_{j_e j_a} \mathbf{w}'_\beta \mathbf{w}'_\delta = \left(\frac{\omega_0}{\omega_D}\right)^2 \Bigg\{ & \frac{1}{2}(\mathbf{1} + \mathbf{zz}) + \frac{\epsilon_0}{2}[(\mathbf{n}_\beta\mathbf{n}_\beta + \mathbf{n}_\delta\mathbf{n}_\delta) + \mathbf{z}\cdot(\mathbf{n}_\beta\mathbf{n}_\beta + \mathbf{n}_\delta\mathbf{n}_\delta)\cdot\mathbf{z}\mathbf{1} + \mathbf{z}\cdot(\mathbf{n}_\beta\mathbf{n}_\beta + \mathbf{n}_\delta\mathbf{n}_\delta)\mathbf{z} + \mathbf{z}(\mathbf{n}_\beta\mathbf{n}_\beta + \mathbf{n}_\delta\mathbf{n}_\delta)\cdot\mathbf{z}] \\ & + \frac{\epsilon_0^2}{2}[(\mathbf{n}_\beta\cdot\mathbf{n}_\delta)(\mathbf{z}\cdot\mathbf{n}_\beta\mathbf{n}_\delta\cdot\mathbf{z}\,\mathbf{1} + \mathbf{n}_\beta\mathbf{n}_\delta + \mathbf{z}\mathbf{n}_\delta\mathbf{n}_\beta\cdot\mathbf{z} + \mathbf{z}\cdot\mathbf{n}_\delta\mathbf{n}_\beta\mathbf{z}) + \mathbf{z}\cdot(\mathbf{n}_\beta\mathbf{n}_\beta\mathbf{n}_\delta\mathbf{n}_\delta + \mathbf{n}_\delta\mathbf{n}_\delta\mathbf{n}_\beta\mathbf{n}_\beta + \mathbf{n}_\beta\mathbf{n}_\delta\mathbf{n}_\delta\mathbf{n}_\beta \\ & + \mathbf{n}_\delta\mathbf{n}_\beta\mathbf{n}_\beta\mathbf{n}_\delta)\cdot\mathbf{z}] + \frac{\epsilon_0}{2}[\mathbf{z}\cdot\mathbf{n}_\beta\mathbf{n}_\beta\mathbf{z} + \mathbf{z}\mathbf{n}_\delta\mathbf{n}_\delta\cdot\mathbf{z} + (\epsilon_0 - 1)\mathbf{z}\cdot(\mathbf{n}_\beta\mathbf{n}_\beta\mathbf{n}_\beta\mathbf{n}_\beta + \mathbf{n}_\delta\mathbf{n}_\delta\mathbf{n}_\delta\mathbf{n}_\delta)\cdot\mathbf{z}] \\ & + \frac{\epsilon_0^2}{2}[4\mathbf{z}\cdot(\mathbf{n}_\beta\mathbf{n}_\beta\mathbf{n}_\delta\mathbf{n}_\delta)\cdot\mathbf{z} + (\epsilon_0 - 1)(\mathbf{n}_\beta\cdot\mathbf{n}_\delta)\mathbf{z}\cdot(\mathbf{n}_\beta\mathbf{n}_\beta\mathbf{n}_\beta\mathbf{n}_\delta + + \mathbf{n}_\beta\mathbf{n}_\beta\mathbf{n}_\delta\mathbf{n}_\beta + \mathbf{n}_\delta\mathbf{n}_\beta\mathbf{n}_\delta\mathbf{n}_\delta + \mathbf{n}_\beta\mathbf{n}_\delta\mathbf{n}_\delta\mathbf{n}_\delta)\cdot\mathbf{z}] \\ & + \frac{\epsilon_0^2}{4}\mathbf{z}\cdot(\mathbf{n}_\beta\mathbf{n}_\beta\mathbf{n}_\delta\mathbf{n}_\delta)\cdot\mathbf{z}[3 + 2(\epsilon_0 - 1) + (\epsilon_0 - 1)^2(\mathbf{n}_\beta\cdot\mathbf{n}_\delta)^2] \Bigg\}. \end{aligned} \quad \text{(A12)}$$

The orientational average of the dyadic (A12) is

$$\mathsf{W}'_m \equiv \left\langle \sum_{j_e j_a} \mathbf{w}'_\beta \mathbf{w}'_\delta \right\rangle . \tag{A13}$$

The averaged dyadic (A13) is the same for any pair $(\beta\delta)$ in the set Λ_m, so the partial sum (2.45) becomes

$$\left\langle \mathbf{x}_+ \cdot \left[\sum_{(\beta\delta)\in\Lambda_m} \sum_{j_e j_a} \mathbf{w}'_\beta \mathbf{w}'_\delta \right] \cdot \mathbf{x}_- \right\rangle = g_m \mathbf{x}_+ \cdot \mathsf{W}'_m \cdot \mathbf{x}_- . \tag{A14}$$

To evaluate Eq. (A13), we need, in addition to the averaged dyads (A7) and (A8), the averaged tetrads which occur in Eq. (A12), for example $\langle \mathbf{n}_\beta \mathbf{n}_\beta \mathbf{n}_\delta \mathbf{n}_\delta \rangle$. We note that

$$\mathbf{n}_\beta = \sqrt{\frac{4\pi}{3}} \sum_q (-1)^q \boldsymbol{\xi}_q Y^\beta_{1,-q} = -\sqrt{4\pi} \{ \boldsymbol{\xi} \otimes Y^\beta_1 \}_{00} . \tag{A15}$$

Here the spherical harmonic is $Y^\beta_{1,-q} = Y_{1,-q}(\theta_\beta, \phi_\beta)$, where the colatitude angle θ_β and azimuthal angle ϕ_β specify the direction of $\mathbf{n}_\beta$.

In Eq. (A15) we have used the tensor-coupling notation of the outstanding reference book by Varshalovich, Moskalev, and Khersonskii,[26]

$$V_{LM} = \{ T_{L_1} \otimes U_{L_2} \}_{LM} = \sum_{M_1 M_2} T_{L_1 M_1} U_{L_2 M_2} C^{LM}_{L_1 M_1 L_2 M_2} \tag{A16}$$

to denote the coupling of two spherical tensors $T_{L_1 M_1}$ and $U_{L_2 M_2}$ to an irreducible product tensor V_{LM} with total angular momentum quantum number L and azimuthal quantum number M. Here $C^{LM}_{L_1 M_1 L_2 M_2}$ is a Clebsch-Gordan coefficient. For example, in Eq. (A15) the irreducible product tensor $\{\boldsymbol{\xi} \otimes Y^\beta_1\}_{00}$ with $L=0$ and $M=0$ is formed from the products of tensor components $\boldsymbol{\xi}_q$, with $L_1=1$ and $M_1=q$, and tensor components $Y_{1,-q}(\theta_\beta, \phi_\beta) = Y^\beta_{1,-q}$, with $L_2=1$ and $M_2=-q$.

As an illustrative example, we evaluate $\langle \mathbf{n}_\beta \mathbf{n}_\beta \mathbf{n}_\delta \mathbf{n}_\delta \rangle$. We first use Eq. (A15) to recouple the dyad $\mathbf{n}_\beta \mathbf{n}_\beta$ with $9j$ coefficients[26]

$$\begin{aligned} \mathbf{n}_\beta \mathbf{n}_\beta &= 4\pi (\{\boldsymbol{\xi} \otimes Y^\beta_1\}_0 \otimes \{\boldsymbol{\xi} \otimes Y^\beta_1\}_0)_{00} \\ &= 4\pi \sum_L (2L+1) \begin{Bmatrix} 1 & 1 & 0 \\ 1 & 1 & 0 \\ L & L & 0 \end{Bmatrix} \\ &\quad \times (\{\boldsymbol{\xi} \otimes \boldsymbol{\xi}\}_L \otimes \{Y^\beta_1 \otimes Y^\beta_1\}_L)_{00} \\ &= -\frac{1}{\sqrt{3}} \{\boldsymbol{\xi} \otimes \boldsymbol{\xi}\}_{00} + \sqrt{\frac{8\pi}{3}} (\{\boldsymbol{\xi} \otimes \boldsymbol{\xi}\}_2 \otimes Y^\beta_2)_{00} . \end{aligned} \tag{A17}$$

In evaluating Eq. (A17) we used the value $1/(3\sqrt{2L+1})$ for the $9j$ coefficient,[26] and we also made use of the well-known recoupling identity for spherical harmonics of the same arguments[26]

$$\{ Y_{L_1} \otimes Y_{L_2} \}_{LM} = \sqrt{\frac{(2L_1+1)(2L_2+1)}{4\pi(2L+1)}} C^{L0}_{L_1 0 L_2 0} Y_{LM} . \tag{A18}$$

Note that the orientational average of the tensor

$$V_{JM}(LL') = \{ \{ \boldsymbol{\xi} \otimes \boldsymbol{\xi} \}_L \otimes \{ \boldsymbol{\xi} \otimes \boldsymbol{\xi} \}_{L'} \}_{JM} \tag{A19}$$

formed from the unit vectors $\boldsymbol{\xi}_m$ is

$$\begin{aligned} \langle V_{JM}(LL') \rangle &= \sum_{M'} \frac{V_{JM'}(LL')}{8\pi^2} \\ &\quad \times \int d\phi \sin\theta \, d\theta \, d\psi D^J_{M'M}(\phi, \theta, \psi) \\ &= V_{00}(LL) \delta_{LL'} \delta_{J0} \delta_{M0} . \end{aligned} \tag{A20}$$

We can use $6j$ or $9j$ coefficients where needed to recouple the product of $\mathbf{n}_\beta \mathbf{n}_\beta$ of Eq. (A17) with the analogous expression for $\mathbf{n}_\delta \mathbf{n}_\delta$ to obtain a superposition of tensors like Eq. (A19). Then, using Eq. (A20) to retain only the rotationally invariant terms in the average, we find that

$$\begin{aligned} \langle \mathbf{n}_\beta \mathbf{n}_\beta \mathbf{n}_\delta \mathbf{n}_\delta \rangle &= \frac{1}{3} \{ \boldsymbol{\xi} \otimes \boldsymbol{\xi} \}_{00} \{ \boldsymbol{\xi} \otimes \boldsymbol{\xi} \}_{00} \\ &\quad + 2\frac{\sqrt{5}}{15} (\{ \boldsymbol{\xi} \otimes \boldsymbol{\xi} \}_2 \otimes \{ \boldsymbol{\xi} \otimes \boldsymbol{\xi} \}_2)_{00} P_2 . \end{aligned} \tag{A21}$$

Here and subsequently, Legendre polynomials without explicit arguments are assumed to have the argument $\mathbf{n}_\beta \cdot \mathbf{n}_\delta = \cos\theta_m$. In deriving Eq. (A21) we made use of the addition formula for spherical harmonics with different arguments[26]

$$\{ Y_L(\mathbf{n}_\beta) \otimes Y_L(\mathbf{n}_\delta) \}_{00} = (-1)^L \frac{\sqrt{2L+1}}{4\pi} P_L(\mathbf{n}_\beta \cdot \mathbf{n}_\delta) . \tag{A22}$$

In like manner, we find that

$$\begin{aligned} \langle \mathbf{n}_\beta \mathbf{n}_\beta \mathbf{n}_\beta \mathbf{n}_\delta \rangle &= \langle \mathbf{n}_\beta \mathbf{n}_\beta \mathbf{n}_\delta \mathbf{n}_\beta \rangle = \langle \mathbf{n}_\delta \mathbf{n}_\beta \mathbf{n}_\delta \mathbf{n}_\delta \rangle = \langle \mathbf{n}_\beta \mathbf{n}_\delta \mathbf{n}_\delta \mathbf{n}_\delta \rangle \\ &= \left[\frac{1}{3} \{ \boldsymbol{\xi} \otimes \boldsymbol{\xi} \}_{00} \{ \boldsymbol{\xi} \otimes \boldsymbol{\xi} \}_{00} \right. \\ &\quad \left. + 2\frac{\sqrt{5}}{15} (\{ \boldsymbol{\xi} \otimes \boldsymbol{\xi} \}_2 \otimes \{ \boldsymbol{\xi} \otimes \boldsymbol{\xi} \}_2)_{00} P_2 \right] \mathbf{n}_\beta \cdot \mathbf{n}_\delta . \end{aligned} \tag{A23}$$

and

$$\begin{aligned} \langle \mathbf{n}_\beta \mathbf{n}_\delta \mathbf{n}_\delta \mathbf{n}_\beta \rangle &= \frac{1}{3} \{ \boldsymbol{\xi} \otimes \boldsymbol{\xi} \}_{00} \{ \boldsymbol{\xi} \otimes \boldsymbol{\xi} \}_{00} (\mathbf{n}_\beta \cdot \mathbf{n}_\delta)^2 \\ &\quad + \frac{\sqrt{3}}{6} (\{ \boldsymbol{\xi} \otimes \boldsymbol{\xi} \}_1 \otimes \{ \boldsymbol{\xi} \otimes \boldsymbol{\xi} \}_1)_{00} |\mathbf{n}_\beta \times \mathbf{n}_\delta|^2 \\ &\quad + \frac{\sqrt{5}}{45} (\{ \boldsymbol{\xi} \otimes \boldsymbol{\xi} \}_2 \otimes \{ \boldsymbol{\xi} \otimes \boldsymbol{\xi} \}_2)_{00} [5 + P_2] . \end{aligned} \tag{A24}$$

To evaluate the nested dot products needed for Eq. (A14) we use Eqs. (A21), (A23), and (A24) to derive the following identities:

$$\mathbf{x}_+ \cdot \{\mathbf{z} \cdot \langle \mathbf{n}_\beta \mathbf{n}_\beta \mathbf{n}_\delta \mathbf{n}_\delta \rangle \cdot \mathbf{z}\} \cdot \mathbf{x}_- = \frac{2}{15} P_2 ; \tag{A25}$$

$$\mathbf{x}_+ \cdot \{\mathbf{z} \cdot \langle \mathbf{n}_\beta \mathbf{n}_\beta \mathbf{n}_\beta \mathbf{n}_\delta \rangle \cdot \mathbf{z}\} \cdot \mathbf{x}_- = \frac{2}{15} P_1 ; \tag{A26}$$

$$\mathbf{x}_+ \cdot \{\mathbf{z} \cdot \langle \mathbf{n}_\beta \mathbf{n}_\delta \mathbf{n}_\delta \mathbf{n}_\beta \rangle \cdot \mathbf{z}\} \cdot \mathbf{x}_- = \frac{2}{9} - \frac{4}{45} P_2 . \tag{A27}$$

Using Eqs. (A12), (A13), (A25), (A26), and (A27) we find

$$\begin{aligned} \mathbf{x}_+ \cdot \mathsf{W}'_m \cdot \mathbf{x}_- = \left(\frac{\omega_0}{\omega_D} \right)^2 \Bigg\{ & 1 + \frac{\epsilon_0}{2} \left[\frac{8}{3} \right] + \frac{\epsilon_0^2}{2} \left[\frac{8}{9} + \frac{88}{90} P_2 \right] \\ & + \frac{\epsilon_0}{2} \left[\frac{4(\epsilon_0 - 1)}{15} \right] \\ & + \frac{\epsilon_0^2}{2} \left[\frac{8(\epsilon_0 - 1) + 8(2\epsilon_0 + 1) P_2}{45} \right] \\ & + \frac{\epsilon_0^2}{4} \left[\frac{2}{15} \left(\frac{2(\epsilon_0 - 1)^2}{15} + \frac{11\epsilon_0^2 + 20\epsilon_0 + 32}{21} P_2 \right. \right. \\ & \left. \left. + \frac{12}{35} (\epsilon_0 - 1)^2 P_4 \right) \right] \Bigg\} . \end{aligned} \tag{A28}$$

To facilitate verification of Eq. (A28), the quantities in square brackets are given in the same order as those of the dyadic (A12), from which they are obtained.

Collecting coefficients of the Legendre polynomials, we rewrite Eq. (A28) as

$$\begin{aligned} \mathbf{x}_+ \cdot \mathsf{W}'_m \cdot \mathbf{x}_- = & \left(\frac{\omega_0}{\omega_D} \right)^2 \left\{ \left(1 + \frac{3\epsilon_0}{5} + \frac{\epsilon_0^2}{15} \right)^2 + \frac{11\epsilon_0^2 (\epsilon_0 + 6)^2 P_2}{630} \right. \\ & \left. + \frac{2\epsilon_0^2 (\epsilon_0 - 1)^2 P_4}{175} \right\} = \left(\frac{\omega_0}{\omega_D} \right)^2 \sum_l c'_l(\epsilon_0) P_l , \end{aligned} \tag{A29}$$

which, together with Eq. (A14), completes the proof of Eqs. (2.45) and (2.46).

The expressions derived here are appropriate for polycrystalline samples of xenon ice, which at present seems to be the only form used for nuclear magnetic resonance. However, it is straightforward to generalize the set averages to single crystals with arbitrary orientations to the applied magnetic field $\mathbf{B}_0$. Instead of the average (A4) over the full rotation group, one can use an average $\langle f \rangle = (48)^{-1} \Sigma_G G f$ over the 48 elements G of the point group O_h, the full symmetry group of the cube. From products of the irreducible representations of O_h one can find unit representations for which the group average is nonzero, in analogy to Eq. (A20). For the paramagnetic antishielding, the rate calculated for the single crystal depends weakly on the orientation of the crystal with respect to the externally applied magnetic field $\mathbf{B}_0$, but for the spin-rotation interaction the calculated rate is exactly the same whether the point group O_h is used for a single crystal or the full rotation group is used for a polycrystalline sample.

*Present address: American Institute of Physics, College Park, MD 20740.
†Present address: McKinsey & Co., Washington, DC 20004.
‡Present address: Harvard–Smithsonian Center for Astrophysics, Cambridge, MA 02138.

[1] N. Bloembergen, *Nuclear Magnetic Relaxation* (Benjamin, New York, 1961).
[2] N. F. Ramsey, Phys. Rev. **78**, 699 (1950).
[3] M. R. Baker, H. M. Nelson, J. A. Leavitt, and N. F. Ramsey, Phys. Rev. **121**, 807 (1961).
[4] E. R. Hunt and H. Y. Carr, Phys. Rev. **130**, 2302 (1963).
[5] H. C. Torrey, Phys. Rev. **130**, 2306 (1963); I. Oppenheim, M. Bloom, and H. C. Torrey, Can. J. Phys. **42**, 70 (1964).
[6] D. Fox, Senior thesis, Princeton University, 1991.
[7] J. van Kranendonk, Physica (Amsterdam) **20**, 781 (1954).
[8] R. E. Norberg, in *Rare Gas Solids*, edited by G. Höhler (Springer-Verlag, New York, 1984); W. W. Warren and R. E. Norberg, Phys. Rev. **148**, 402 (1966).
[9] D. Raftery, H. Long, T. Meersmann, P. J. Grandinetti, L. Reven, and A. Pines, Phys. Rev. Lett. **66**, 584 (1991); D. Raftery, H. Long, L. Reven, P. Tang, and A. Pines, Chem. Phys. Lett. **191**, 385 (1992).
[10] M. Gatzke, Ph.D. thesis, Princeton University, 1992.
[11] M. Gatzke, G. D. Cates, B. Driehuys, D. Fox, W. Happer, and B. Saam, Phys. Rev. Lett. **70**, 690 (1993).
[12] D. M. TonThat, M. Ziegeweid, Y.-Q. Song, E. J. Munson, S. Appelt, A. Pines, and J. Clarke, Chem. Phys. Lett. **272**, 245 (1997).
[13] G. D. Cates, D. R. Benton, M. Gatzke, W. Happer, K. C. Hasson, and N. R. Newbury, Phys. Rev. Lett. **65**, 2591 (1990).
[14] H. M. McConnel and C. H. Holm, J. Chem. Phys. **25**, 1289 (1956).
[15] J. R. Lyerla, D. M. Grant, and R. D. Bertrand, J. Phys. Chem. **75**, 3967 (1971).
[16] Z. Wu, T. G. Walker, and W. Happer, Phys. Rev. Lett. **54**, 1921 (1985).
[17] F. J. Adrian, Phys. Rev. **136**, A980 (1964).
[18] L. I. Yastrebov and A. A. Katsnelson, *Foundations of One-Electron Theory of Solids* (Mir, Moscow, 1987).
[19] I. I. Rabi, N. F. Ramsey, and J. Schwinger, Rev. Mod. Phys. **26**, 167 (1954).
[20] E. Clementi and C. Roetti, At. Data Nucl. Data Tables **14**, 177 (1974).
[21] N. C. Bacalis, D. A. Papaconstantopoulos, and W. E. Pickett, Phys. Rev. B **38**, 6218 (1988).
[22] J. Lurie, J. L. Feldman, and G. K. Horton, Phys. Rev. **150**, 180 (1966).
[23] N. D. Bhaskar, W. Happer, and T. McClelland, Phys. Rev. Lett. **49**, 25 (1982); G. D. Cates *et al.*, Phys. Rev. A **45**, 4631 (1992).
[24] E. R. Andrew, *Nuclear Magnetic Resonance* (Cambridge University Press, New York, 1958), p. 47.
[25] M. Goldman, *Spin Temperature and NMR in Solids* (Oxford University Press, New York, 1970).
[26] D. A. Varshalovich, A. N. Moskalev, and V. K. Khersonskii, *Quantum Theory of Angular Momentum* (World Scientific, Singapore, 1988).